FLOWS IN CURVED DUCTS AND DIFFUSERS- EXPERIMENTAL INVESTIGATIONS AND COMPUTATIONS

by

JOHN ARUL G.

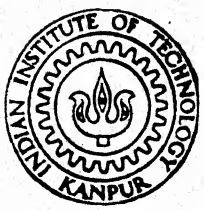

DEPARTMENT OF AEROSPACE ENGINEERING

INDIAN INSTITUTE OF TECHNOLOGY KANPUR

MAY, 1991

FLOWS IN CURVED DUCTS AND DIFFUSERS - EXPERIMENTAL INVESTIGATIONS AND COMPUTATIONS

A Thesis submitted
in partial fulfilment of the Requirements
For the Degree of

MASTER OF TECHNOLOGY

By

JOHN ARUL. G

to the

Department of Aerospace Engineering
Indian Institute of Technology Kanpur

May, 1991

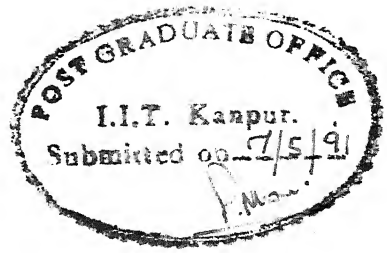

CERTIFICATE

This is to certify that the thesis entitled

Flows in curved ducts and annular diffusers - Experimental investigations and computations

is a record of the work carried out under my supervision and that it has not been submitted elsewhere for awarding a degree.

7.5.91

(R. K. SULLEREY)
Professor
Dept. of Aerospace Engineering
Indian Institute of Technology,
Kanpur

ACKNOWLEDGEMENTS

I am extremely grateful to Professor R. K. Sullerey for suggesting me the topic and for inspiring and guiding me throughout the course of this work.

I am grately indebted to Mr. V.C. Srivastava for all his help during the various stages of this work. I am thankful to Mr. K.S. Mudappa for lending me the furness control manometer.

I am thankful to Mr. J.B. Mishra for his help in the experimental set up and in measurements. I wish to express my thanks to Mr. Bhattacharya and Mr. Santhraj for their help during fabrication. I am thankful to Mr. A.K. Srivastava for his help in typing this report.

John Arul G.

CONTENTS

NAME : JOHN ARUL G.

ROLL NO. : 8910108

TITLE OF THE THESIS : FLOWS IN CURVED DUCTS AND DIFFUSERS-EXPERIMENTAL INVESTIGATIONS AND COMPUTATIONS.

THESIS SUPERVISOR : Dr. R. K. SULLEREY
PROFESSOR
DEPT. OF AEROSPACE ENGINEERING
I.I.T. KANPUR

ABSTRACT

The present study is aimed to investigate the flow behaviour in two-dimensional ducts with curvature and divergence angle in a range typical of two-dimensional air intakes.

A detailed experimental investigation of the mean flow characteristics in the core flow and in the two-dimensional turbulent boundary layers over the inner and outer wall of the 3 degree curved diffuser and the curved duct having a ratio of the radius of curvature to the semiwidth of the duct of 6 is carried out.

The measured data include wall static pressures,potential flow velocity profiles (both radial and spanwise), boundary layer profiles, wall shear stress and flow angularity measurements. Experimental results provide information on static pressure recovery, growth of boundary layer with turning

angle, flow separation, flow field distortions and secondary flows.

Improvement in pressure recovery for a 4^{o} semi divergence angle diffuser was obtained using a set of two pyramid type vortex generators on the inner wall.

The pressure and velocity distributions in the curved duct and curved diffusers were calculated using a streamline curvature method. Computed results are compared with experimental data with and without including the displacement effects of the boundary layer.

The boundary layer thickness and wall shear stress have been calculated using a non-iterative integral method. Computed results are compared with the experimental data.

NOMENCLATURE

R = Streamline radius of curvature

r = Half-width of the duct, diffuser

l = Height of the duct, diffuser

P = Static pressure'

ρ = Density

U = Free stream velocity at the inlet of the duct/diffuser

C_P = Static pressure coefficient

h_1, h_2, h_3, h_4, h_5 = Manometer reading at the respective hole in the five hole probe.

K_δ, K_ψ = Inclination factors

δ = Pitch angle within the vertical equational plane

ψ = Yaw angle within the horizontal meridian plane

} Only for five hole probe measurements.

U_τ = Skin friction velocity

Y = Distance from the wall

ν = Kinematic viscosity

ΔP_P = Preston tube reading

d = Diameter of the preston tube

τ_w = Wall shear stress

$$x^* = \log_{10}\left(\frac{\Delta P_P\, d^2}{4\rho\, \nu^2}\right)$$

$$y^* = \log_{10}\left(\frac{\tau_w\, d^2}{4\rho\, \nu^2}\right)$$

C_f = Skin friction coefficient

A, B = Constants

U_s = Streamwise velocity component

U_n = Normal velocity component

P_o = Stagnation pressure

ψ = Streamfunction or mass flow

s = Distance in the streamwise direction

n = Distance normal to streamline

δ = Boundary layer thickness

m = Boundary layer profile exponent

$\mu_{eff} = \mu + \mu_t$ = Effective viscosity

μ = Laminar viscosity

μ_t = Turbulent viscosity

F = Head's entrainment function

$H_1 = \dfrac{\delta - \delta_1}{\delta_2}$ = Shape factor

$H_2 = \dfrac{\delta_1}{\delta_2}$ = Shape factor

$\delta_1 = \int_o^{\delta} \left(1 - \dfrac{U_s}{U_{se}}\right) dn$ = Displacement thickness

$\delta_2 = \int_o^{\delta} \dfrac{U_s}{U_{se}} \left(1 - \dfrac{U_s}{U_{se}}\right) dn$ = Momentum thickness

Re = Reynolds number

G = Constant for secondary flow

ω = Width of the duct, diffuser

Subscripts

S = Streamwise direction

n = Normal direction

e = Edge of boundary layer

w = Wall

LIST OF FIGURES

FIG NUMBER

Chapter - 1

INTRODUCTION

The function of the air intake is to supply subsonic flow at entry into the compressor. Even in supersonic flight the flow should be reduced to the specified entry Mach number for the compressor. The permissible Mach number at compressor entry is generally limited in the range of 0.5 - 0.6.

For modern combat aircraft the intake is generally through side or ventral air inlets adjacent to the fuselage. Here the intake is strongly influenced by adjacent parts of the fuselage and even subject to considerable disturbance during some conditions of flight. Because of the space limitation and arrangement of other components, the intake ducts have curvature and divergence simultaneously.

The two-dimensional rectangular intake is considerably less sensitive to oblique flows. Many modern combat aircrafts are having two dimensional air intakes.

The deceleration of flow should be conducted in a way that optimum increase in pressure over a wide operating range is achieved with minimum flow distortion at the compressor inlet. The performance of the diffuser is generally evaluated in terms of the pressure recovery. Because of the adverse pressure gradient, secondary flow and several other reasons, the inner wall boundary layer thickness increases rapidly. If the flow turning is continued, the flow separates. This separtion results in

excessive pressure loss and non-uniformity in flow distribution resulting in a serious loss in engine performance.

1.1 Literature Survey:-

Fox and Kline [1] have systematically investigated the flow regimes of curved diffusers. They concluded that the flow regimes can be described in terms of inlet length to width ratio, area ratio and the turning angle. The turning angle variations in their investigations was from 0 to 90 degrees.

Sagi and Johnston [2] have developed the methodology for the design of two dimensional curved diffusers. They have found out that the inner wall is subjected to the following curvature induced effects (i) Increased potential flow loadings along the wall, (ii) Reduced turbulent mixing along the wall, (iii) Increased thickness of the inner wall boundary layer caused by secondary flows off end walls.

So and Mellor [3] have investigated the turbulent boundary layer flows with both uniform and adverse pressure distributions along convex and concave walls having 150 degrees turning angle with strong curvature. They have shown that the ability of the flow to support adverse pressure gradient along the convex wall is reduced and hence the flow separates earlier than the corresponding plane flow. They have found that the secondary flow becomes significant, because of the rapid growth of the boundary layer thickness near separtion. Conversely, the flow over concave wall supports more adverse pressure gradient without

separation than a parallel flow. It was shown that on the outer wall, the boundary layer at the position of the trough of the wave is approximately twice as thick as the boundary layer at the position of the crest of the wave. They have indicated a reduced log law region for both the strong convex and concave curvatures.

Eskinazi and Yeh [4] have conducted the experimental investigations on a curved channel having a turning angle of 150 degrees and strong curvature with zero pressure gradient. They have found that the turbulence intensities were greater near the concave wall than that near convex wall. They have shown that there is considerable deviation from the logarithmic law of the wall for both the flows over convex and concave surfaces.

Ellis and Joubert [5] have conducted experimental investigations on a curved channel having a turning angle of 230 degrees and strong curvature with zero and favourable pressure gradient. They have presented a modified form of the law of the wall for curved surfaces. They have shown that the usual log law applies over a very small region. They have found that the C_f decreases along the convex wall, but it increases or decreases slightly for small or large radius of curvature respectively along the concave wall. Their results indicate that the turbulence is suppressed on the convex wall and amplified on the concave wall.

Meroney and Bradshaw [6] have tested for mild curvature cases having zero pressure gradient. They have found that the mixing rate is more on the concave wall than on the convex wall. They have observed the presence of longitudinal vortices on the

outer wall flow. They have presented a modified form of the law of the wall for both the convex and concave surfaces. C_f was found to decrease slightly along the convex wall whereas it was found to increase slightly along the concave wall.

Ramaprian and Shivaprasad [7] have investigated over surfaces having mild longitudinal curvatures with zero pressure gradients. They have found that the region close to the wall was not affected by the wall curvature, but the outer region was very sensitive to even mild curvature. They have indicated a reduced log law region for both the convex and concave walls. C_f was found to decrease along the convex wall, while it decreases slightly along the concave wall.

Smits et.al.[8] have used short bends to investigate the impulse response of the boundary layer. They have observed that the boundary layer thickness is a minimum at the crest (max. in C_f) and a maximum at the trough (min. in C_f).

Bandopadhay [9] in his review paper has stated that the C_f of the flow on the convex wall dropped to levels lower than that would occur on the flow on the flat plate. He has also stated that research was going on to evaluate the potential of a convex surface curvature to offer a net drag reduction.

Srinivasa Rao [10] has conducted experimental investigations for the diffuser having a semi-divergence angle of 6^{o}. He has concluded that the flow separates between 15 to 30 degree on the inner wall resulting in non-uniform velocity

profiles afterwards.

Sullerey [11] has conducted experimental investigations for the diffusers having a semi-divergence angle of 3, 4, 5 and 6 degrees. He has concluded that the diffuser having a semi-divergence angle of 3 degree has a good pressure recovery with less flow distortion when compared to the diffusers having more divergence angles.

Goenka et. al [12] have shown that if a pyramid shaped insert was attached to the diverging wall of a two-dimensional diffuser, it generated a transverse pressure gradient that caused the incoming flow to roll up into two symmetric vortices, which replaced the separated regions along the diffuser expansion wall. They concluded that the static pressure recovery was improved with less flow distortion.

Isomoto and Honami [13] have done experimental investigations on reducing the reattachement length in a backward facing step. They have observed that if a rod of 5mm dia was placed at the edge of the boundary layer there was a local increase in turbulence intensity. This was found to shorten the reattachment length. They have also tried to shorten the reattachement length with a cavity on the wall.

There are two methods in simulating the fluid flow by mathematical models. The first and the accurate method is, to solve the complete Navier-Stokes equation. But this is computationally very complex. The second method is, to solve the

potential flow, boundary layer flow and secondary flow problems separately. The potential flow analysis can be carried out by methods such as the streamline curvature method. For simulating the boundary layer and secondary flows, some empirical formulae can be used. When compared to the first the second approach is easier.

The theory underlying the streamline curvature method has been described by R.A. Novak [14]. He has tried this method for some axisymmetric cases such as the flow through compressor and turbine blades. He has suggested that it can be used for some non-axisymmetric cases also.

Wilkinson [15] has used both the normal and tangential quasi-orthogonals to the flow. He has experimented this method for some axisymmetric cases. He has shown that using tangential quasi orthogonals, compressible flows can be predicted more accurately.

Bindon and Carmichael [16] have presented the SCM method using normals to the flow. They have used this for calculating the subsonic and supersonic flows in the axial turbine blades. This method is used for calculating the semi-three dimensional flow because it incorporates the variation in flow height (flare) in the equations without taking into account the z-momentum equation.

Andrew [17] has shown that SCM can be adapted to calculate the non-axisymmetric flows in a thin meridional sector

of a regenerative turbomachine. He has used quasi-orthogonals to the flow.

Schumann [18] has proposed an analytic model to calculate the three-dimensional axisymmetric turbulent flow field in a radial vaneless diffuser. The model is based on the assumption that the radial and tangential boundary layer profiles be approximated by power-law profiles.The integrated radial and tangential momentum and continuity equations for the boundary layer and corresponding inviscid equations for the core flow were solved using a Runge-kutta techniques.

Pourahmadi and Humphrey [19] have used the k-ε model of turbulence to predict the developing two-dimensional, curved channel flows. Here an expression which accounts simultaneously for the effects of streamline curvature and pressure strain is incorporated in the turbulent viscosity expression.

1.2 Scope of present work :-

Literature review shows that for strong and mild curvatures lot of experimental data is available. For intermediate curvature these was a need for more experimental data. Here detailed experimental investigations have been carried out for intermediate curvature.

The present experimental investigations were conducted on a two-dimensional curved diffuser and a curved duct both having a turning angle of 95.5 degrees, at a Reynolds number of 7.8×10^5. The curved channels have a ratio of radius of curvature

based on channel width as 6 and a length of duct based on channel width as 5.

Previous investigation by Sullerey [11] have confirmed that the diffuser having a semi-divergence angle of 3 degree is having less pressure loss and flow disortion. Therefore it was decided to carryout detailed investigations for 3 degree diffuser. Vortex generators were kept on the inner wall for both the diffusers having a semi divergence angle of 3^{o} and 4^{o}. This was done to see the effect of vortices in postponing separation and in improving the pressure recovery.

Performance curves like pressure coefficient, velocity profiles and boundary layer profiles were plotted at various radial locations. The friction coefficient variations were also plotted at different radial stations along the length of the duct and diffuser. Flow angularity distributions were compared for the duct and the diffuser.

All the experiments were conducted with a flow having uniform velocity profile at the inlet to both curved diffuser and curved duct.

Pressure distributions were calculated using the Streamline Curvature Method developed by Bindon and Carmichael [16]. Boundary layer flows were predicted using the power law approximations for the boundary layer velocity profiles.

It is expected that the results of the present work would be useful in the design of subsonic curved ducts of aircraft intakes.

Chapter - 2

EXPERIMENTAL PROGRAMME

2.1 Description of Wind Tunnel :-

The tunnel used in the present investigations is an open circuit blower type low speed wind tunnel. Air from the 22 KW blower after passing through the contraction of area ratio 10:1, entered the test section. The blower has a shutter arrangement near the eye of the fan, which provides for the control of airspeed ranging from a minimum of 25 m/s to a maximum of 54 m/s at 25^{o}C and at atmospheric pressure. The Reynolds number range corresponding to these speeds is 7.8×10^{5} to 1.29×10^{6} .

2.2 Description of the experimental set up :-

The test section consisted of an initial straight duct of approximately 2.5 ft. long and a curved duct of approximately 6.2 ft long. The initial straight section was used for getting a fully developed, zero pressure gradient turbulent boundary layer at inlet to the test section.

The duct and diffuser had an inlet rectangular cross section of 381 x 305 mm. The curved duct and the curved diffuser had a R/r = 6 and L/2r = 5. The total turning angle of the duct is 95.5^{o} . The length L is taken as the arc length corresponding to mean radius R = 114.3 cm. The duct width, 2r is 381 mm. The inner and outer walls were made of 5 mm thick perspex sheet for smooth working surface. The top and bottom walls were made of 12

mm thick plywood.

Wall static pressure tappings were provided at 5^{o} intervals on the bottom, inner and outer walls of the diffuser. Six slots of 30 cm x 1.2 cm were provided at 15^{o} interval for detailed flow measurement at these stations. For curved duct these slots were provided at an interval of 10^{o} . For boundary layer measurements, holes of 6 mm diameter were made on the inner and outer wall so that boundary layer velocity profile could be obtained at different stations. Fig. 1 and 2 gives the geometry of the curved duct and curved diffuser respectively.

2.3 Measurement Technique, Instrumentation and Testing Technique:

The velocity profile at the inlet of the duct/diffusers was obtained using a 3 mm diameter standard pitot static probe.

Static pressure measurements were taken on the inner, outer and bottom walls. For all measurements, the reference pressure as measured by a pressure tapping located at the centre of the straight duct before the ducts/diffusers. The static pressure coefficient was calculated according to relation

$$C_P = \frac{P - P_{ref}}{1/2\ \rho U^2}$$

where 'U' is the free stream velocity at the inlet of the duct/diffuser.

For velocity measurements, three types of probes were used. First is a pitot-disc probe combination as shownin Fig. 3. This

was generally used for measuring the velocity in the core region outside the inner and outer wall boundary layers. For measurements of velocity profile within the boundary layer, two pitot probes were designed one for the inner and the other for the outer wall as shown in Fig. 3.

Flow angularity measurement :-

The five hole probe as shown in Fig. 4 was used to measure the flow angularity. The probe head has five holes of 0.5 mm diameter. One of these holes is centrally positioned and the other four are all situated at 45^{o} from the central hole. They are arranged two by two in perpendicular planes, whose intersections line coincide with the central hole and is also the axis of the probe. The five holes are connected through the stainless steel and flexible tubes to the manometer.

The probe was aligned perpendicular to a particular radial direction and the manometer readings for five holes were noted for every change in the z-direction. The inclination factors K_{ψ} and K_{δ} , which are dependent on probe head geometry and relative flow stream directions were obtained from these measurements. They are defined, below

$$K_{\delta} = \frac{h_1 - h_2}{h_1 - h_4} = f(\delta, \psi)$$

and

$$K_{\psi} = \frac{h_1 - h_3}{h_1 - h_5} = f(\delta, \psi)$$

From the calibration curves as shown in Figs 5 and 6, got from Sullerey's [11] report, the values of δ and ψ were obtained. These are useful in determining the direction of the velocity vector in two cartesian angles, one the yaw angle (ψ) within the horizontal meridian plane and the other the pitch angle (δ) within the vertical equational plane.

Wall Shear Stress Measurements :-

For wall shear measurements Preston tube was used. The Preston tube as shown in Fig. 3 is nothing but a simple pitot tube resting on the surface. It is based on the assumption of the law of the wall ($U/U_\tau = f(U_\tau Y/\nu)$ common to the boundary layers and fully developed flow. The difference between the pressure recorded by the Preston tube and the undisturbed static pressure can be expressed in the non-dimensional form

$$\frac{\tau_\omega d^2}{4\rho \nu^2} = F_1\left[\frac{\Delta P_p d^2}{4\rho \nu^2}\right]$$

where ΔP_p is the preston tube reading (i.e. the difference between pitot and static pressures), d is the diameter of the preston tube, τ_ω is the wall shear stress, ρ is the fluid density and ν the kinematic viscosity of the fluid.

Patel [20] has calibrated the tube and has found out that the function F1 is different for different regions.

In the region

$$1.5 < y^* < 3.5$$

$$5.6 < (U_\tau\, d/2\nu) < 55$$

the empirical formulae is given by

$$y^* = 0.8287 - 0.1381\ x^* + 0.1437 x^{*2} - 0.0060\ x^{*3}$$

and in the region

$$y^* < 1.5$$

$$(U_\tau\ d/2\nu) < 5.6$$

the empirical formula is

$$y^* = 1/2\ x^* + 0.037$$

where $x^* = \log_{10}\left[\frac{\Delta\rho_\rho\ d^2}{4\rho\ \nu^2}\right]$ and $y^* = \log_{10}\left[\frac{\tau_\omega\ d^2}{4\rho\ \nu^2}\right]$

The coefficient of friction was calculated according to the formula

$$C_f = \frac{\tau_\omega}{1/2\ \rho U^2}$$

where `U' is the free stream velocity at the inlet of the duct/diffuser.

The validity of the law of the wall is restricted to values of $U_\tau\ y/\nu$ less than some upperlimit. This is dependent on the type of flow, the pressure gradient and possibly the upstream history of the flow. The function f is different for different regions.

For the linear sublayer

$$U/U_\tau = U_\tau\ y/\nu$$

and for a fully turbulent region, it is

$$U/U_\tau = A \log_{10} \left(U_\tau \, y/\nu \right) + B$$

where A and B are constants.

Patel [20] has shown that in adverse pressure gradients, preston tubes of increasing diameter shows a wrong value. This is because of the early departure of the velocity distribution from the usual logarithmic law. Small diameter tubes are desirable. In this investigation 0.8 mm diameter tube was used. This was provided at 5, 15, 30, 45, 50 and 60 degrees on the inner and outer walls of the curved diffuser. It was kept at an interval of 10^{o} upto 80 degrees on the inner and outer walls of the curved duct.

A grid was placed at the exit to the tunnel nozzle for increasing the free stream turbulence. The diameter of the wires used to form the mesh is 1.5 mm. It was also placed at the inlet to the 3^{o} diffuser to see the effect of increased free stream turbulence at the two different places.

A rod of 6 mm diameter was placed at different angular locations in the inner wall boundary layer region. This was done to see the effect of free stream turbulence in postponing separation and improving the pressure recovery.

The vortex generator (curved pyramid) as shown in Fig 7 was kept on the inner wall at different places to study the effect of generated longitudinal vortices in postponing separation and in improving the pressure recovery.

For pressure and velocity measurements Furness type FC012 model 1 digital micromanometer with 20 channels was used. Dweyer gauge manometer was also used for some of the measurements.

Chapter - 3

EXPERIMENTAL RESULTS AND DISCUSSIONS

In the first part the results of experimental investigations which have been carried out in curved rectangular ducts of R/r ratio of 6 are presented. Next, the experimental results for 3^{o} diffuser having a R/r ratio of 6 are discussed. Finally, the experimental results of the 4^{o} diffuser with vortex generator are presented.

Fig. 8 shows the C_p distribution in the curved duct for R/r ratio of 6. Due to curvature effects, there is a low pressure trough in the inner wall pressure distribution and the pressure is high along the outer wall. Sullerey [11] has stated that the potential flow velocity profile shows a peak value near the inner wall and that it decreases along the radius towards the outer wall. He has also stated that the angular momentum values were constant in the radial direction. The inner wall boundary layer thickness increases rapidly with flow turning. The outer wall boundary layer is thin compared to the inner wall. Boundary layer velocity measurements were taken in the mid span region.

Fig 9 shows that C_f on the inner wall of the curved duct increases marginally upto 20^{o} turning angle and subsequently decreases upto 50^{o} turning angle. It again shows an increase thereafter. On the contrary the C_f along the outer wall increases slightly. The curve is a bit wavy.

Fig 10 shows the static presssure distribution for the

diffuser of semidivergence angle 3^{o}. The presence of a low pressure trough in the inner wall pressure distribution curve at the beginning of curvature is a result of the adjustment of the flow from the zero pressure gradient prevailing across the straight section (before the curved diffuser) to the radial pressure gradient existing in the curved diffuser. After the low pressure trough, the static pressure rises continuously on the inner wall. The difference in the outer wall and inner wall static pressures decreases with increase in turning.

The values of C_p at the inner, centre and outer tappings for the 3^{o} diffuser after 15^{o}, 30^{o}, 45^{o} and 75^{o} turning angles are given in the Table 1.

		C_p distribution		
S.No.	Ang. locations	Inner	Centre	Outer
1.	15	- 0.17	0.11	0.34
2.	30	- 0.01	0.22	0.44
3.	45	0.12	0.32	0.50
4.	75	0.30	0.42	0.57

The measurements were taken in the mid span region.

Figs. 11 to 13 show the radial velocity profiles for the 3^{o} diffuser at 15^{o}, 30^{o} and 45^{o} turning angles. It is evident from these figures that the inner wall boundary layer thickness grows rapidly. The values of the boundary layer displacement thickness are 0.02ω, 0.027ω and 0.062ω at 15^{o}, 30^{o} and 45^{o} turning

angles respectively. The outer wall boundary layer displacement thickness does not show much variation with the turning angle.

Velocity profile after a turning angle of 60^{o} is shown in Fig. 14. It is observed that the flow is separated at 60^{o} turning angle spanwise velocity profiles at 60^{o} and 75^{o} turning angles are shown in Figs. 15 and 16. It is evident from these figures that the flow is highly distorted in the mid span region after 60^{o} turning angle. Much of flow distortion is in the inner wall region. The outer wall boundary layer is well behaved.

The top and bottom wall boundary layer thickness increases in the downstream direction in the 3^{o} diffuser. The average of the top and bottom wall displacement thickness at 30^{o} and 45^{o} turning angles are 0.018H and 0.0285H respectively.

3.1 Effect of Inlet Condition:-

A grid was placed infront of the straight duct and 3^{o} diffuser to see the effect of free stream turbulence in the diffuser. The grid consists of two stainless steel tubes each of 1.5 mm diameter spanning the entrance of the straight duct on both inner and outer side. The spacing between the wall and the first tube and the first and second tubes is 3 mm.

From the Fig. 17 it is evident that the pressure recovery of the diffuser is more or less the same as that of the diffuser without the grid. However the flow separation along the inner wall is postponed somewhat and the flow is also less distorted when compared to the diffuser without grid as shown in

ig. 18.

It was observed that when the same grid was placed at he inlet to the diffuser, the pressure recovery of the diffuser lecreased. These results are not presented here.

3.2 Details of boundary layer measurements:-

Fig. 19 shows the C_f distribution on the inner wall and outer wall for the 3^o diffuser. C_f decreases along the inner wall. It is slightly above zero at 50^o turning angle and at 60^o turning angle it goes to zero. This confirms that the flow separates in between the 50^o and 60^o turning angle. C_f increases slightly upto 15^o turning angle of the outer wall. From then onwards it decreases marginally in the downstream direction.

Figs. 20 and 21 show the mean velocity profiles on the convex (inner) and concave (outer) walls of the 3^o diffuser plotted in the inner layer coordinates. It can be seen that near the wall the experimental data for both the convex and concave walls generally agree with the log law

$$U/U_\tau = 5.6 \log_{10} \left(\frac{y U_\tau}{\nu} \right) + 5.5$$

as that of the flat wall.

The range of the log law region is $1600 < y^* < 3800$ for the convex wall at 15^o turning angle. At 30^o turning angle the values are much higher than the log law line. The range of the log law region is $800 < y^* < 2500$ for the concave wall at 15^o

ırning angle. Subsequently at other stations in the downstream irection, generally the values are below the log law line. These ɔservations are in general agreement with the findings of So and ellor [3] and Ellis and Joubert [5].

Fig. 22 shows the mean velocity profiles on the concave ıall plotted in the inner layer coordinate of the 3^{o} diffuser with ɡrid infront of the straight duct.

3.3 Flow angularity measurements:-

The five hole probe was aligned such that the y and z-directions were respectively the radial and spanwise direction. The x-direction is the tangential direction. Measurements have been carried out at 60^{o} and 75^{o} turning angles of the 3^{o} diffuser. Distribution of flow angle ψ is shown in Fig. 23 at the 60^{o} turning angle. The angle ψ has positive values for the bottom and top walls indicating movement of wall boundary inner layer fluid towards the inner wall due to the radial pressure gradient. In the midspan region, the angle has a negative value indicating secondary motion from inner to outer wall. The value of this angle is - 13^{o} in this direction. The maximum value of radial velocity is about 25% of the tangential velocity. The measurements were carried out at radial stations at 0.3ω, 0.5ω and 0.7ω from the inner wall.

The variation of spanwise flow angle δ is shown in Fig. 24. The angle varies from - 8 to + 8 degrees. The maximum value of spanwise velocity is 15% of the tangential velocity.

The value of the angle ψ is -3^{o} in the midspan region in ıe curved duct. Flow angularity measurements taken in the curved ɹct show that the secondary flow is significantly less in the uct when compared to the 3^{o} diffuser.

.4 Effect of the Vortex generator:-

Goenka et al. [12] in their experimental investigations ɔn two dimensional diffusers used a pyramid-shaped vortex ɟenerator to the basic diffuser's expansion wall. The upsweep on the pyramid upper surface creates a transverse presssure gradient which causes the incoming flow to form two symmetric longitudinal vortices along the pyramid side surfaces. They have also shown that the separated regions were eliminated by the pyramid. The flow was less distorted and this has improved the pressure recovery of the diffuser.

A similar type of vortex genertor in the shape of a curved genertor in the shape of a curved pyramid as shown in Fig. 7 was attached to the inner wall of the curved diffuser with varying trailing edge height.

To avoid mechanical difficulties in the preliminary investigations, the vortex generator did not cover the entire inner wall upto the point of separation. The curved pyramid covered 22^{o} turning angle. The measurements were taken after placing it at different angular locations on the inner wall of the diffuser. This curved pyramid shaped insert generated longitudinal vortices which replaced the separated regions on the

ıner wall of the diffuser.

From the Fig. 25 it is evident that when the vortex enerator having a ratio of trailing edge height to boundary layer hickness of 1.16 was attached to the inner wall from 38^{o} - 60^{o} urning angle of the 3^{o} diffuser, the pressure recovery was almost ;ame as that of the diffuser without the vortex generator. Fig. :6 shows that the performance of the 3^{o} diffuser was more or less the same when the pyramid was placed at two locations on the inner wall. One from 0^{o} to 22^{o} turning angle and the other from 38^{o} to 60^{o} turning angle. In both the cases the ratio of the trailing edge height to the boundary layer thickness is 1.16.

Fig. 27 shows the C_p distribution of the 3^{o} diffuser when a pyramid having a ratio of trailing edge height to boundary layer thickness of 1.18, attached to the inner wall from 33^{o} - 55^{o} turning angle. It indicates that there is a moderate decrease in the pressure recovery of the diffuser with pyramid compared to the diffuser without pyramid. Fig. 28 shows the C_p distribution of the 3^{o} diffuser with pyramid attached to the inner wall from 38^{o}-60^{o} turning angle. It has a ratio of trailing edge height to boundary layer thickness of 1.11. It can be seen from the figure that there is a slight decrease in the pressure recovery of the diffuser with pyramid, compared to the diffuser without pyramid.

From this we can conclude that there is an optimum height of the vortex generator vis-a-vis the boundary layer thickness. Due to limited experiments, this optimum value could not be obtained. Physically it appears that while the presence of

ortex generator delays separation, it has losses of its own due o the vortex dissipation. Thus for 3^{o} diffuser, where separtion osses are not so high, the gain in pressure recovery due to /ortex generator is only marginal.

Fig. 29 shows the C_p distribution in the 4^{o} diffuser with two vortex generators kept simultaneously at two locations on the inner wall. One from 0^{o} to 22^{o} turning angle and the other from 33^{o} to 55^{o} turning angle. In both the cases the ratio of the trailing edge height to boundary layer thickness is 1.11. It is clear from the figure that the pressure recovery of the diffuser has improved. In the peak region the average C_p values of the diffuser with pyramid is 20% higher than that of the diffuser without pyramid. Figs. 30 and 31 show the radial and spanwise velocity profiles at the 60^{o} location of the 4^{o} diffuser with vortex generator kept as before. Fig. 31a shows the spanwise velocity profile at the 60^{o} location of the 4^{o} diffuser without vortex generator. The radial velocity profiles were taken in the midspan region. It can be seen from the Fig. 30 that the extent of separation is less in the diffuser with vortex genertor when compared to the diffuser without vortex generator.

Isomoto and Honami [13] in their experimental investigations have placed a rod of 5 mm diameter at the edge of the boundary layer, upstream of the reattachment length. They have observed that the local increase of turbulence intensity near the edge of the boundary layer has shortened the reattachment length.

With the motivation to increase free stream turbulence in the outer edge of the boundary layer, a rod of 6 mm was placed near the edge of the inner wall boundary layer at different angular locations. The free stream turbulence created by the rod delayed the separation. However there was in general a reduction in the pressure recovery due to losses created by presence of the rod.

Chapter - 4

INVISCID FLOW ANALYSIS

STREAMLINE CURVATURE METHOD

In the present streamline curvature method, streamline coordinate system for a two-dimensional and two-directional flow is followed. The coordinate lines are the streamlines(s) and the normal lines(n). The n-lines are perpendicular to the streamlines and point toward their centre of curvture. Although the s-lines and n-lines are always perpendicular to each other, the s and n directions are variable because the streamlines are not straight. The major advantage with this system is that the velocity at any point is always parallel to the s direction. We can write the velocity vector

$$\vec{U} = U_s \vec{s} + U_n \vec{n} = U_s \vec{s} \quad (U_n = 0) \qquad (1)$$

The method is termed the streamline curvature method (SCM) because the equations of motion are used in a form which relates the streamwise velocity gradient directly to the radius of curvature of the streamline.

4.1 Equations of Motion :-

It is assumed that the total pressure is constant along streamlines, that is

$$\frac{DP_o}{Dt} = 0$$

This means that the energy equation and the streamwise momentum equation are automatically satisfied. Here instead of considering the z-momentum equation, the variation in height

(flare) is incorporated in the other momentum and continuity equation. Thus only the normal momentum equation and the continuity equation have to be solved numerically.

For incompressible, frictionless, steady, and semi-three-dimensional (flared) flow, the equations of motion are

$$1 = \frac{-R}{U}\frac{\partial U}{\partial n} \qquad (2)$$

and

$$\frac{\partial \psi}{\partial n} = \rho U l \qquad (3)$$

For numerical purposes, these two equations are combined and written in the finite difference form

$$\Delta U = \frac{-\Delta \psi}{\rho l R} \qquad (4)$$

where R is streamline radius of curvature, U is velocity, n is distance normal to streamline, ψ is stream function or mass flow, ρ is density and l is particle height normal to the plane of flow. (See Appendix for derivation).

4.2 Boundary conditions for incompressible flow:-

These equations are used for solving the incompressible flows. In a subsonic (elliptic) procedure, the curvature at a point should be a function of flow data from upstream and downstream. The initial and final streamlines are defined by channel boundaries. This is shown in the figure below.

4.3 Boundary collocation streamline curvature procedure:-

Here the method of boundary collocation between one channel and bounding streamline is used.

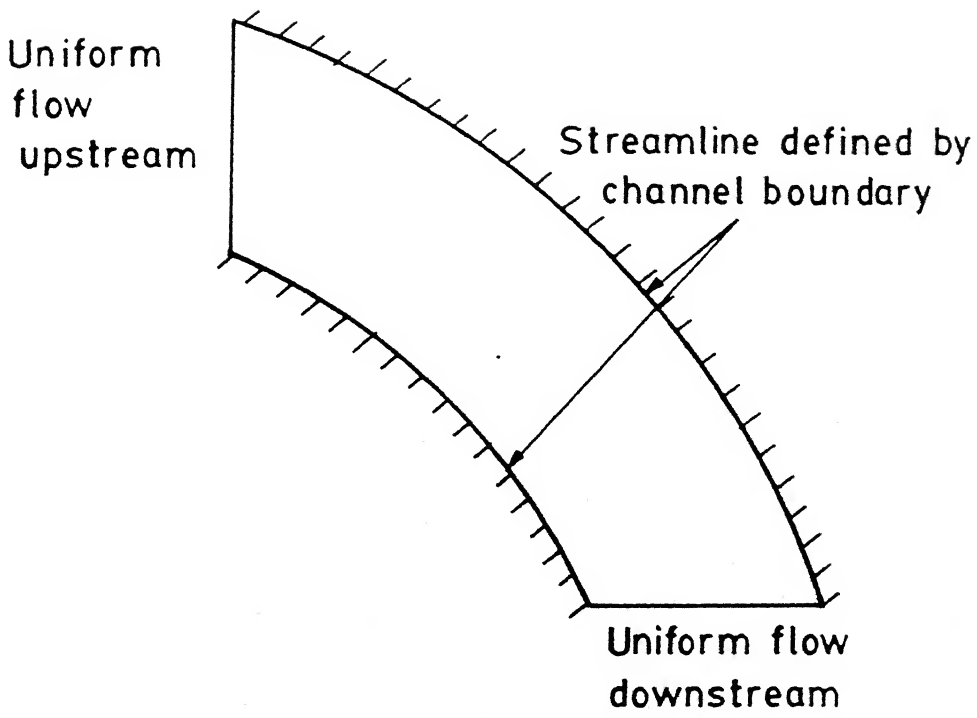
Uniform
flow
upstream
Streamline defined by
channel boundary
Uniform flow
downstream

A velocity distribution is assumed along one channel boundary, termed the commencing surface. Here the streamlines curvature is circular. Using the initial velocity and surface curvature along the boundary, equation (3) and (4) were used to find the velocity and location of the first streamline at each point. All the points are fitted by an approximating curve. Each time taking one point upstream and one point downstream to a particular point to fit a curve. The streamline curvature is calculated at every station for the first streamline and the equations are applied in a similar fashion to find the second streamline. By repeating this process sequentially all the streamlines are produced (or stacked) until the final or flow bounding streamline is reached. The final streamline will not coincide with the second channel surface, the terminating surface unless the assumed velocity distribution was correct. An iterative loop is set up whereby the initial velocity distribution is changed according to the deviation of the final streamline from the terminating surface and the process is repeated until the two geometries coincide.

The channel mass flow is adjusted to give the final streamline and terminating surface coincidence at each normal where the calculations were carried out.

The result were obtained with the fourth order Runge Kutta method which used the data at one point to determine the finite difference step to be taken at that point.

The entire procedure is as shown in Fig. 32.

The present treatment is flexible regarding channel shape. There is a link between the shape of the final streamline and the commencing surface velocity distribution, which is included in the convergence procedure.

BOUNDARY LAYER ANALYSIS

The flow field near the walls in a curved duct is extremely complex since the flow is turbulent, unsteady, viscous and three-dimensional.

In the present case, a two-dimensional calculation procedure for turbulent flows in a curved duct is presented. The method is a noniterative integral method. It is much faster than the finite difference methods. The primary assumption made is that the tangential or the streamwise boundary layer velocity profile can be described by power law.

4.4 Analysis :-

The following assumptions are made for the boundary layer flow analysis.

i) The flow is steady and turbulent everywhere.

ii) The fluid is a perfect gas.

iii) The flow is incompressible.

iv) The boundary layer velocity profile in the streamwise direction may be described by the power law.

$$\frac{U_s}{U_{se}} = \left[\frac{n}{\delta}\right]^m \qquad (5)$$

The boundary layer equations of motion in streamline coordinates for turbulent flow are as follows:

Continuity

$$\frac{R}{R+n}\frac{\partial U_s}{\partial s} + \frac{\partial U_n}{\partial n} + \frac{U_n}{R+n} = 0 \qquad (6)$$

Streamwise Momentum

$$\frac{R}{R+n}U_s\frac{\partial U_s}{\partial s} + U_n\frac{\partial U_s}{\partial n} + \frac{U_n U_s}{R+n} = \frac{-R}{R+n}\frac{1}{\rho}\frac{\partial p}{\partial s} +$$

$$\frac{\mu_{eff}}{\rho}\left\{\frac{1}{R}\frac{\partial U_{se}}{\partial n} - \frac{U_{se}}{R^2} + \frac{\partial^2 U_{se}}{\partial n^2}\right\} \qquad (7)$$

Radial Momentum

$$\frac{\partial p}{\partial n} = \frac{\rho U_{se}^2}{R} \qquad (8)$$

If the power law profile of equation (5) is assumed, the problem reduced to that of determining the free-stream velocity component U_{se}, normal velocity component U_{ne}, the boundary layer thickness δ, the boundary layer profile exponent m and the free stream pressure P. Thus five equations are needed to solve the flow field.

Two of these equations are obtained by integrating equations (6) and (7) through the boundary layer which results in the following equations after making suitable approximations.

Assuming $R >> n$

$$\int_0^{\delta}\frac{\partial U_s}{\partial s}\,dn + \int_0^{\delta}\frac{\partial U_s}{\partial s}\,dn + \int_0^{\delta}U_n\,d_n = 0 \qquad (9)$$

$$\int_0^{\delta} U_s \frac{\partial U_s}{\partial s}\, dn + \int_0^{\delta} U_n \frac{\partial U_s}{\partial s}\, dn + \int_0^{\delta} \frac{U_s U_n}{R}\, dn = \frac{1}{\rho} \int_0^{\delta} \frac{\partial p}{\partial s}\, dn +$$

$$\frac{1}{\rho} \left\{ \int_0^{\delta} \mu_{eff} \frac{\partial U_s}{\partial n}\, dn + \int_0^{\delta} \mu_{eff} \frac{\partial^2 U_s}{\partial n^2}\, dn \right\} \qquad (10)$$

For the core flow, from the radial momentum equation and the energy equation one more equation is obtained.

$$\frac{\partial U_{se}}{\partial n} = \frac{U_{se}}{R} \qquad (11)$$

The channel continuity equation is given by

$$\frac{\partial \psi}{\partial n}\, \delta n = \delta U1\, \delta n \qquad (12)$$

Combining equations (12) and (11) we get

$$\frac{\partial U}{\partial \psi} = - \frac{1}{\rho 1 R} \qquad (13)$$

Equations (12) and (13) were used in the streamline curvature method for the inviscid flow. Instead of calculating P and U_{se} again and complicting the problem further, the values of P and U_{se} were taken from the previously computed values.

4.5 The Entrainment Function :-

One additional equation is needed to solve this system since an additional unknown is added in the integration of equations (6) and (7), i.e., the normal velocity at the edge of the boundary layer, U_{ne} . This can be modelled using Head's entrainment relation which empirically predicts the rate at which

fluid from the free stream is entrained into the boundary layer. Head [21] showed that the entrainment rate can be modelled as a function only of a boundary layer shape factor. Sumner and Shanebrook [22] extended the definition to three-dimensional, incompressible turbulent flows as follows:

$$F = \frac{1}{U_{se}} \left(U_{se} \frac{d\delta}{ds} - U_{ne} \right) = 0.0306 \, (H_1 - 3)^{-0.653} \quad (14)$$

where H_1 is the shape factor.

Since the inner wall boundary layer grows rapidly the power constant, - 0.653 holds good for the inner wall. But the outerwall boundary layer thickness is almost constant and so only a constant of - 3.0 will predict the growth. The value - 3.0 signifies that there is less entrainment.

Along the inner wall there is another factor which is causing the thickening of the boundary layer i.e., the secondary flow. This is dependent on the tangential velocity, flow turning angle and $\frac{dU}{dZ}$. Approximately this is expressed as some constant multiplied by the flow turning angle.

4.6 The Skin-friction Coefficient :-

Expressions for wall shearing stress can be given by

$$\tau_{sw} = \frac{\rho U_{se}^2}{2} C_f \quad (15)$$

where C_f is given by the Ludweig-Tillman relation which is

$$C_f = 0.246 \; Re_{\delta 2}^{-0.268} \; e^{-1.561 \, H_2} \quad (16)$$

Here the Reynolds number is calculated with respect to the momentum thickness. H_2 is the shape factor.

4.7 Final Form of the Equations:-

After simplifying equations (9) and (10) we get

$$\frac{d\delta}{ds} = \frac{2m\delta}{U_{se}} \frac{dU_{se}}{ds} + (1-2m^2)F + \frac{(2m+1)^2}{2} \times$$

$$\left[\frac{\delta C_P}{\partial s} + \tau_{we} + \frac{\tau_{we}\delta}{R} \right] - (1 - 2m^2)\, G + \frac{3Gm(1-m)}{R} \qquad (17)$$

$$\frac{dm}{ds} = \frac{(2m+1)\ (m+1)}{U_{se}} \frac{dU_{se}}{ds} - (2m+1)(m+1)\ m\ F +$$

$$\frac{(2m+1)\ (m+1)^2}{2} \left[\frac{\partial C_P\ \delta}{\partial s} + \tau_{we} + \frac{\tau_{we}\delta}{R} \right] +$$

$$\frac{G}{R} \times (1 + 4m - 3m^2) + \frac{G}{\delta} m(m+1)\ (2m+1) \qquad (18)$$

Equations (17) and (18) were solved for two unknowns (δ and m) using a fourth-order Runge-kutta technique.

The complete derivation of the final form of the continuity equation is described in the Appendix. The streamwise momentum equation is derived similarly.

Initial Conditions:-

The initial value of m should be around 0.2. However δ will be a significant portion of the inlet straight duct exit width. This has to be got from the experimental data.

Chapter - 5

COMPUTED RESULTS AND DISCUSSIONS

SCM was used to calculate the C_p distribution in the curved diffuser and curved duct.

Fig. 33 shows the C_p distribution in 3^o diffuser, comparing the SCM results and the experimental data. Along the inner wall generally the predictions are good upto 45^o turning angle. Near the leading edge the predicted values are lower than the experimental data. In the middle region and along the outer wall also the predictions are good upto 40^o turning angle. After separtion the experimental values are much lower than the computed values. After modifying the channel boundary by incorporating the displacement thickness to the C_p was again calculated. Then the computed values of C_p were much closer to the experimental values upto 45^o turning angle. The streamlines are closely spaced in the inner wall region and they are sparsely spaced in the outer wall region.

Fig. 34 shows the comparison of computed and measured C_p distribution in a 4^o diffuser. Generally the prediction is not very good. Along the inner wall the prediction is good upto 35^o turning angle. The experimental values downstream of that is much less than the computed results. In the middle and in the outer region the experimental values are less than the computed results. After changing the channel boundary by adding the displacement thickness, the predicted C_p values fall much closer to the experimental values upto 45^o turning angle.

The comparison of computed and measured C_p distribution in a 5^o diffusser is given in Fig. 35. Generally the experimental values fall short of the predicted values. Along the inner wall, apart from the initial region, the computed values are close to the experimental values upto 30^o turning angle. In the middle and in the outer region the experimental values are marginally lower than the computed values.

The comparison of computed and measured C_p distribution in the curved duct having a R/r ratio of 6 is shown in Fig. 37. The predicted values fall very close to the computed values along the inner wall and in the middle region. In the outer wall region the experimental values fall marginally short of the computed values upto 60^o turning angle and after that the difference increased in the downstream direction. This difference is because of the thickening of the inner wall boundary layer.

The results from the boundary layer analysis have been compared with the experimental data. Fig. 38 shows the C_f distribution in the curved duct having a R/r ratio of 6. From 10^o to 30^o turning angle along the inner wall the experimental values of C_f is higher than the computed results. From 40^o to 80^o turning angle along the inner wall the agreement is generally good. Though the method predicts the growth of the boundary layer thickness, the prediction is good only upto 20^o turning angle. Downstream of that the prediction is much less than the experiemental values. The power-law exponent increases in the downstream direction along the inner wall. This prediction is good.

It can be seen from the Fig. 38 that there is not much of a difference between computed C_f and the experimental C_f along the outer wall of the curved duct. The computed C_f is marginally lower than the experimental C_f. The growth of the computed boundary layer thickness along the outer wall is in general agreement with the experimental data. The power law exponent increases marginally in the downstream direction along the outer wall, which is also in agreement with the experimental results.

While implementing the integral boundary layer method for curved diffuser, it was observed that Head's entrainment function in the present form underpredicts the growth of boundary layer on the inner wall.

In the real flow situation there is considerable growth of inner wall boundary layer due to secondary flow, a correct modelling of the same is required before accurate predictions can be made using boundary layer prediction methods.

Chapter - 6

CONCLUSIONS

The following conclusions can be drawn from the present experimental investigations carried out in the curved duct and curved diffusers.

i) In the curved duct there is a low pressure trough in the inner wall pressure distribution and the pressure increases from inner to outer wall radially. The free stream velocity profile shows a peak near the inner wall and the velocity decreases in the radial direction such that the angular momentum is conserved.

ii) In the 3 degree semi-divergence diffuser the pressure recovery is good with a low level of flow distortion upto 30 degree turning angle. After the low pressure trough near the entrance, the static pressure rises continuously along the inner wall. The difference in the outer and inner wall static pressures decreases with increase in turning. The free stream velocity profile shows a peak value near the inner wall and the velocity decreases in the radial direction. However the conservation of angular momentum is not fully satisfied for the case of diffuser.

iii) The inner wall boundary layer thickness grows in the downstream direction in the curved duct, while it is almost constant along the outer wall. The skin friction measurements show that there is no separtion upto 80 degree turning angle along both on the inner and outer walls.

iv) In the 3 degree semi-divergence diffuser the boundary layer thickness increases along the inner wall and it separates between 50 degree and 60 degree turning angles. But along the outer wall the boundary layer thickness is almost constant and it does not separate. Only at 15 degree turning angle the logarithmic law of the wall is satisfied. Downstream of that the velocity profiles depart from the log law.

v) Flow angularity measurements show that the strength of the secondary flow is much less for the curved duct when compared to the 3 degree semi-divergence diffuser for the same angular location. At 60 degree turning angle in the mid span region the value of the yaw angle ψ is - 3^{o} in the curved duct, while it is around - 13^{o} in the 3 degree semi-divergence curved diffuser. Similarly the secondary flow velocities are much higher for curved diffusers.

vi) Some Vortex generators in the form of a curved pyramid attached to the inner wall of the 3 degree semi-divergence diffuser delays separation but the pressure recovery of the diffuser remains almost same.

vii) With two Vortex generators simultaneously put on the inner wall between 0 to 22 degrees and 33 to 55 degrees turning angle of a 4 degree semi-divergence diffuser, the average static pressure recovery improved by 20%.

viii) The streamline curvature method predicts the C_p distribution in a 3 degree semi-divergence diffuser with reasonable accuracy. For the 4 degree and 5 degree

semi-divergence diffuser the predictions appears to be reasonable upto 40 degree turning angle. The computed results do not agree with the measured data beyond separation point.

ix) Results using the integral boundary layer method show good agreement with the experimental data for the curved duct both for the inner and outer wall boundary layers. To implement the method for the case of curved diffuser, it is necessary to model entrainment arising due to secondary flow in order to predict well the growth of the boundary layer.

Bibliography

1. Fox, R.W. and Kline, S.J. : Flow regimes of curved subsonic diffusers, J. of Basic Engg. Trans. ASME, series D, Vol. 84 (1962).
2. Sagi and Johnston, J.P. : The design and performance of two-dimensional curved diffusers, J.of Basic Engg. Trans. ASME, series D, Vol. (1969).
3. Ronald, M.C. SO and Mellor : An experimental investigation of turbulent boundary layers along curved surfaces. NACA CR 1940 (1972).
4. Eskinazi, S. and Hsuan Yeh : An investigation on fully developed turbulent flows in a curved channel. J. of Aero Sci., Vol. 23 (1956).
5. Ellis, L.B. and Joubert, P.N. : Turbulent shear flow in curved duct. J. of Fluid Mechanics, Vol. 62 (1974).
6. Meroney, R.N. and Bradshaw, P. : Turbulent boundary-layer growth over a longitudinally curved surface AIAA Journal, Vol. 13 (1975).
7. Ramaprian, B.R. and Shivaprasad, B.G. : Mean flow measurements in turbulent boundary layers along mildly curved surfaces. AIAA Journal, Vol. 15 (1977).
8. Smits, A.J., Young, S.T.B. and Bradshaw, P. : The effect of short regions of high surface curvature on turbulent boundary layers. J.of Fluid Mechanics, Vol. 94 (1979).

9. Bandyopadhyay, P.R. : Review - Mean flow in turbulent boundary layers disturbed to alter skin friction. J. of Fluids Engineering, Vol. 108 (1986).

10. Srinivasa Rao, M. : Effect of curvature and diffusion on flow through rectangular ducts, M. Tech thesis (1989).

11. Sullerey, R.K. : Experimental investigations on internal flows in curved diffusers. ADA Funded Project (1990).

12. Goenka,L.N., Panton, R.L. and Bogard, D.G. : Pressure and three-component velocity measurements on a diffuser that generates longitudinal vortices. J. of Fluids Engineering, Vol. 112 (1990).

13. Isomoto, K. and Honami, S. : The effect of inlet turbulence intensity on the reattachment process over a backward - facing step. J. of Fluid Engineering, Vol. 111 (1987).

14. Novak, R.A. : Streamline curvature computing procedures for fluid-flow problems. J. of Basic Engg. Trans. ASME series D (1967).

15. Wilkinson, D.H., : Calculation of blade-to-blade flow in a turbomachine by streamline curvature ARC, R&M 3704 (1970).

16. Bindon, J.P. and Carmichael, A.D. : Streamline curvature analysis of compressible and high mach number cascade flows. J. of Mechanical Engg. Science, Vol. 13 (1971).

17. Andrew, D.N. : The calculation of flow in regenerative turbomachines by a streamline curvature method, Proc. Instn. Mech. Engrs. Vol. 204 (1990).

18. Schumann, L.F. : A three-dimensional axisymmetric calculation procedure for turbulent flows in a radial vanless diffuser. J. of Engg. for Gas Turbines and Power,

Vol. 108 (1986).

19. Pourahmadi, F. and Humphrey, J.A.C. : Prediction of curved channel flow with an extended K-ε model of turbulence, AIAA Journal, Vol. 21 (1983).

20. Patel, V.C. : Calibration of the preston tube and limitations on its use in pressure gradients, J. of Fluid Mechanics, Vol. 23 (1965).

21. Head, M.R. : Entrainment in the turbulent boundary layer. ARC, R & M 3152 (1958).

22. Shanebrook, J.R. and Sumner, W.J. : Entrainment equation for three-dimensional compressible, turbulent boundary layers. AIAA Journal, Vol. 10 (1972).

Appendix 1

Figure shows the fluid particle for derivation of basic equation. Figure a shows the section through particle centre in the plane of flow showing pressure forces acting. Figure b shows the section through particle centre normal to the plane of flow and in the n direction.

The fluid particle is bounded by two streamlines and two normals to the streamlines. The flow is assumed to be steady and inviscid. The fluid particle is subject to pressure forces and centrifugal forces.

The net pressure force acting towards the center of the streamline radius of curvature R, taking into consideration the components of the pressure forces on the six sides is given by

$$\left\{\left[\left(P + \frac{\partial P}{\partial n}\delta n\right) \times (R \times \partial n) \times 1 - P1R\right] - \right.$$

$$\left[\left(P - {}^{1}/_{2}\,\frac{\partial P}{\partial s}\,\partial s + {}^{1}/_{2}\,\frac{\partial P}{\partial n}\,\delta n\right) \times \left(1 - {}^{1}/_{2}\,\frac{\partial 1}{\partial s}\,\delta s\right) \times \frac{\delta n}{2}\right) +$$

$$\left.\left[\left(P + {}^{1}/_{2}\,\frac{\partial P}{\partial s}\,\partial s + {}^{1}/_{2}\,\frac{\partial P}{\partial n}\,\delta n\right) \times \left(1 + {}^{1}/_{2}\,\frac{\partial 1}{\partial s}\,\delta s\right) \times \frac{\delta n}{2}\right)\right]\right\}\delta\theta \qquad (1)$$

by simplifying this equation, we obtain

$$\left\{\frac{\partial P}{\partial n}\,\delta n\, R1 - \frac{1}{2}\,\frac{\partial P}{\partial n}\,\delta n^{2}\right\}\delta\theta = \frac{\partial P}{\partial n}\,\delta n\,\delta\theta\left(R - \frac{\delta n}{2}\right) \qquad (2)$$

where P is pressure, V is velocity, s is distance measured along a streamline, n is distance normal to the streamline and 1 is the height of the fluid particle.

The centrifugal force on the fluid particle is

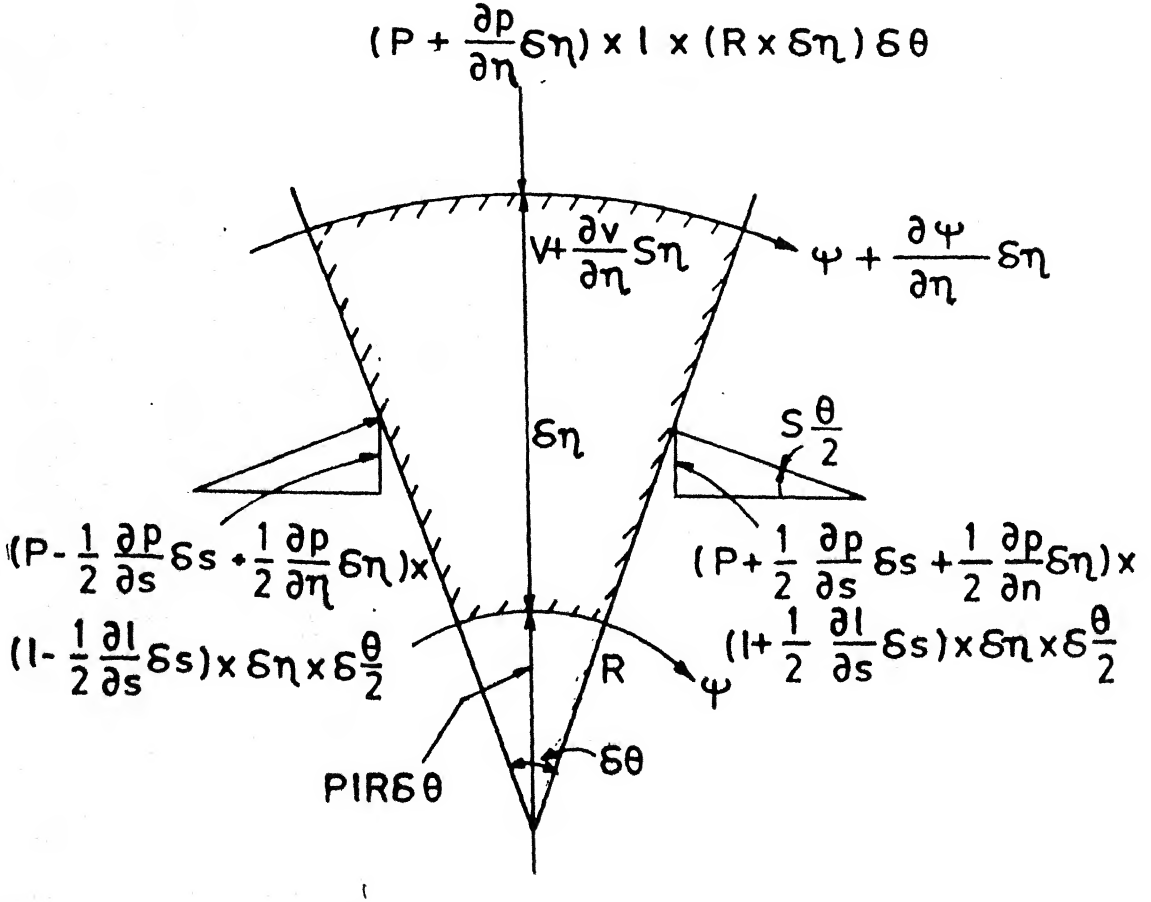
$(P+\frac{\partial p}{\partial \eta}\delta\eta)\times 1\times(R\times\delta\eta)\delta\theta$
$V+\frac{\partial v}{\partial \eta}\delta\eta$
$\psi+\frac{\partial \psi}{\partial \eta}\delta\eta$
$\delta\eta$
$S\frac{\theta}{2}$
$(P-\frac{1}{2}\frac{\partial p}{\partial s}\delta s+\frac{1}{2}\frac{\partial p}{\partial \eta}\delta\eta)\times$
$(1-\frac{1}{2}\frac{\partial l}{\partial s}\delta s)\times\delta\eta\times\delta\frac{\theta}{2}$
$(P+\frac{1}{2}\frac{\partial p}{\partial s}\delta s+\frac{1}{2}\frac{\partial p}{\partial n}\delta\eta)\times$
$(1+\frac{1}{2}\frac{\partial l}{\partial s}\delta s)\times\delta\eta\times\delta\frac{\theta}{2}$
R
ψ
$PIR\delta\theta$
$\delta\theta$
(a)

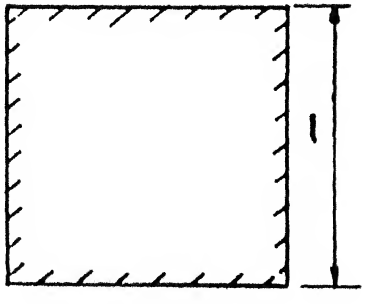
1
(b)

$$\rho \left\{ 1 \times \delta n \times \left(R + \frac{\delta n}{2}\right) \delta\theta \right\} \frac{V^2}{\left(R + \frac{\delta n}{2}\right)}$$

$$= \quad \delta l \; \delta n \; \delta\theta \; V^2 \qquad (3)$$

Equating the pressure force and centrifugal force

$$\frac{\partial P}{\partial n} \; \delta n \; \delta\theta \; 1 \; \left(R - \frac{\delta n}{2}\right) = \rho l \; \delta n \; \delta\theta \; V^2$$

$$\frac{1}{\rho} \frac{\partial P}{\partial n} = \frac{V^2}{\left(R - \frac{\delta n}{2}\right)} \qquad (4)$$

Seeking a substitution for the term $1/\rho \left(\frac{\partial P}{\partial n}\right)$, the energy equation

$$P_o = P + 1/2 \; \rho V^2 \qquad (5)$$

is written as

$$\frac{1}{\rho} \frac{\partial P_o}{\partial n} = \frac{1}{\rho} \frac{\partial P}{\partial n} + V \frac{\partial V}{\partial n}$$

$$- V \frac{\partial V}{\partial n} = \frac{1}{\rho} \frac{\partial P}{\partial n} \left(\frac{\partial P_o}{\partial n} = 0 \right) \qquad (6)$$

substituting equations (6) in (4) and simplifying gives

$$- \frac{\partial V}{\partial n} = \frac{V}{\left(R - \frac{\delta n}{2}\right)} \qquad (7)$$

The continuity equation in the curvilinear co-ordinates used is

$$\frac{\partial \psi}{\partial n} \delta n = \rho V l \; \delta n$$

or

$$\frac{\partial \psi}{\partial n} = \rho V l \qquad (8)$$

where ψ is stream function or mass flow. Equations (7) and (8) are the basic streamline curvature equations. These equations can be written in the finite difference form.

$$\frac{\Delta\psi}{\Delta n} = \rho V l \qquad (9)$$

$$\frac{\Delta V}{\Delta n} = - \frac{V}{(R - \frac{\Delta n}{2})} \qquad (10)$$

where $\Delta\psi$, Δn, Δn and Δl are finite increments taken normal to the streamlines. Combining equations (9) and (10) and rearranging

$$\Delta V = - \frac{\Delta\psi}{l\rho R} \qquad (11)$$

Appendix 2

Perivation of the final form of the continuity equation:-

In order to calculate the duct/diffuser flow field, equations (9) and (10) must be recast as ordinary differential equations.

If Leibnitz' rule is used to interchange differentiation and integration, equation (9) becomes

$$\frac{d}{ds}\int_0^{\delta} U_s\,dn - \frac{d\delta}{ds}\,U_{se} + U_{ne} + \frac{U_{ne}}{R}\,\delta = 0$$

$$\frac{1}{U_{se}}\,\frac{d}{ds}\int_0^{\delta} U_s\,dn + \frac{U_{ne}}{U_{se}}\,\frac{\delta}{R} = \frac{1}{U_{se}}\left[U_{se}\,\frac{d\delta}{ds} - U_{ne}\right] \qquad (1)$$

The term on the right-hand side of equation (1) is Head's entrainment function, F, and will be evaluated later. The integrals can be evaluated for the power-law profiles of equation (5) in chapter 4 which results in the following equation.

$$\frac{1}{U_{se}}\,\frac{dU_{se}}{ds} + \frac{1}{\delta}\,\frac{d\delta}{ds} - \frac{1}{(m+1)}\,\frac{dm}{ds} + \frac{(m+1)}{R}\,\frac{U_{ne}}{U_{se}} = \frac{(m+1)}{\delta}\,F \qquad (2)$$

Using similar techniques, the streamwise momentum equations can also be reduced to ordinary differential equation.

The entrainment function, F, is given by

$F = 0.0306\,(H_1-3)^{-0.653}$. The shape factor, H_1, is defined by the expression

$$H_1 = \frac{\delta - \delta_{1s}}{\delta_{2s}}$$

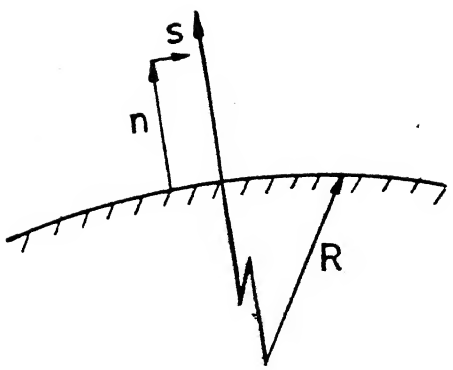

STREAMLINE CO-ORDINATE SYSTEM

Using the power-law profiles of equation (5) in chapter-4

$$\delta_{1s} = \frac{m\delta}{m+1}$$

and

$$\delta_{2s} = \frac{m\delta}{(m+1)(2m+1)}$$

Therefore the shape factor, H_1, becomess

$$H_1 = \frac{1 + 2m}{m}$$

Finally the eentrainment function, F, becomes

$$F = 0.0306 \left(\frac{m}{1-m} \right)^{0.653} .$$

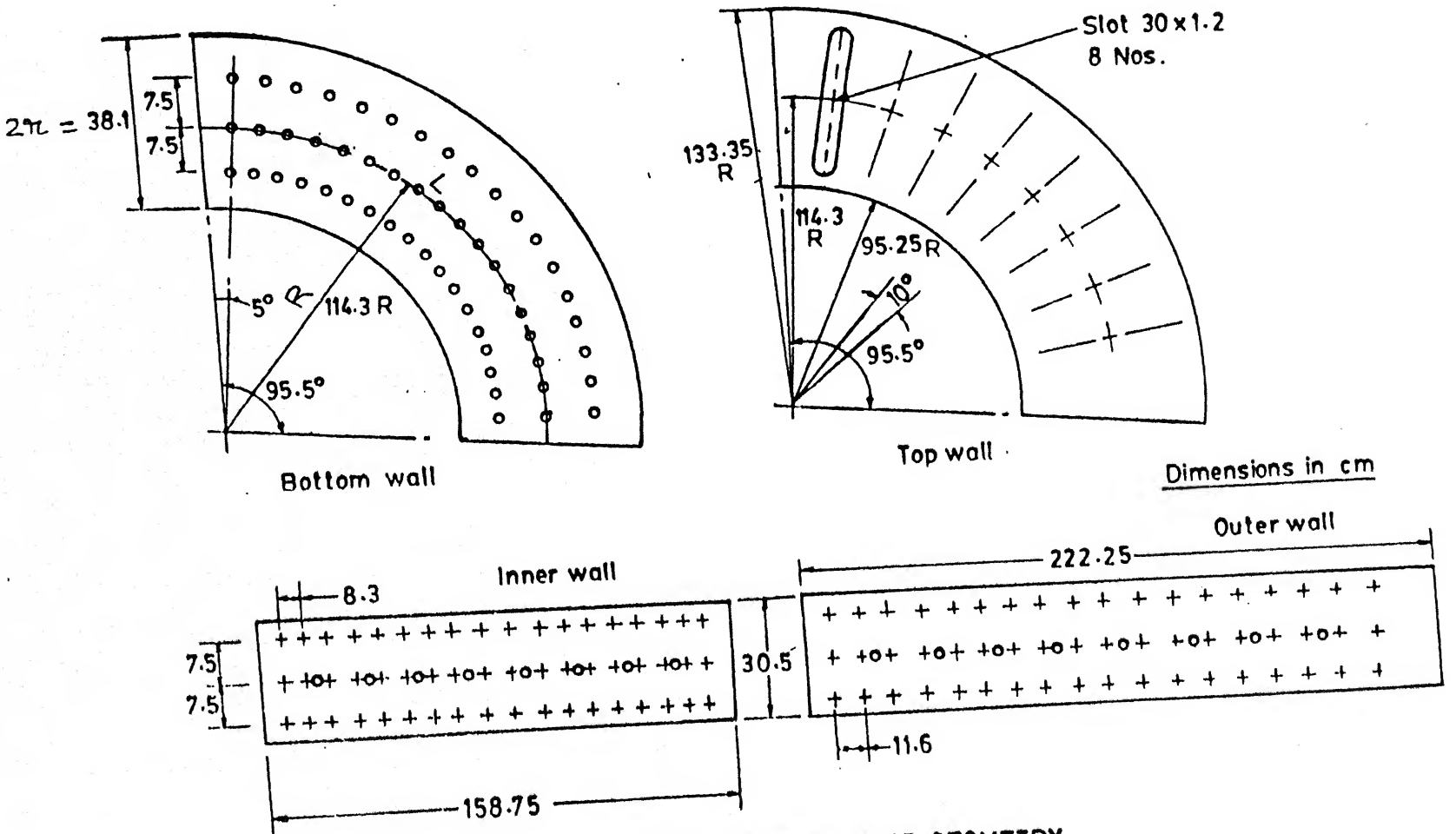

FIG. 1 CURVED DUCT GEOMETRY

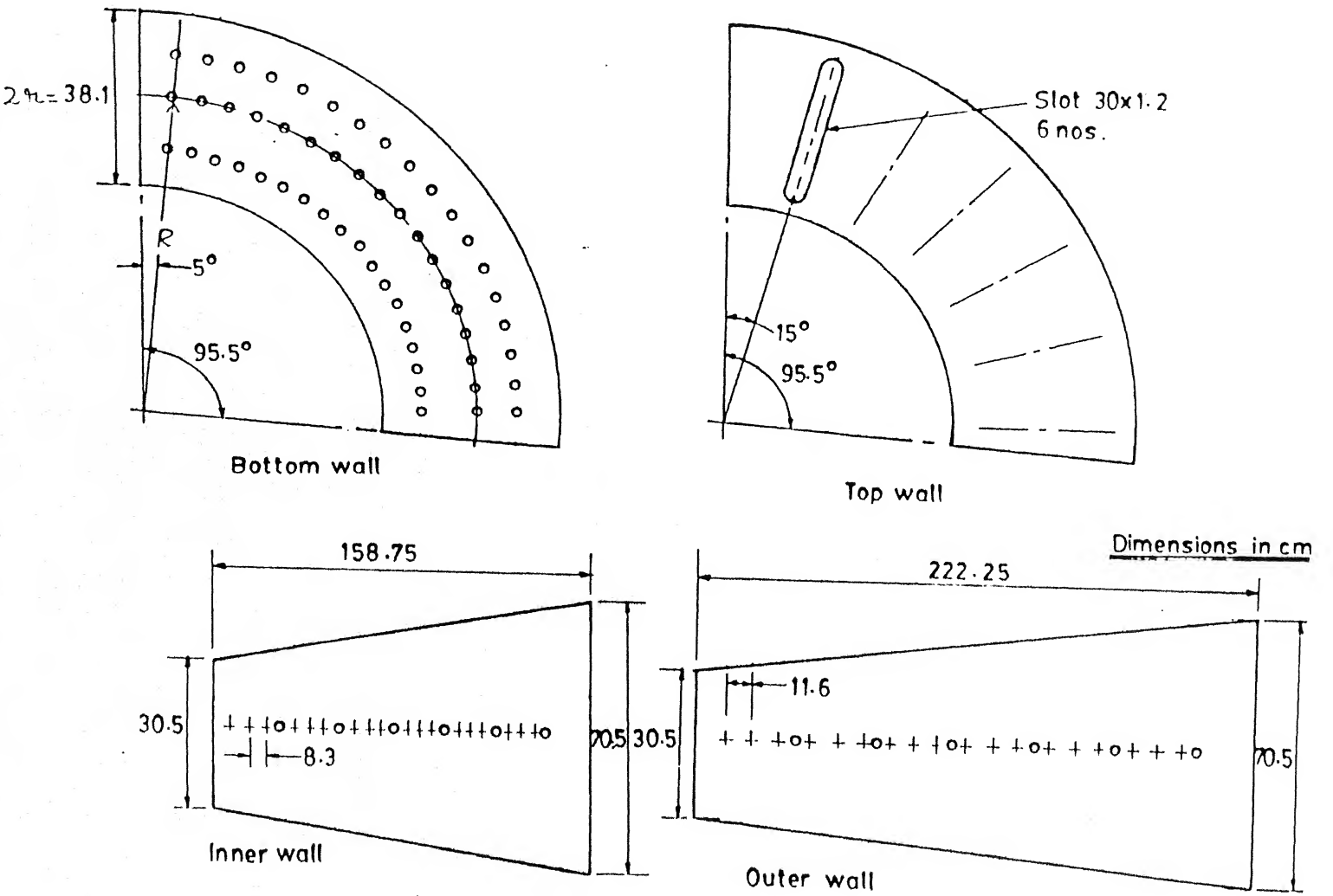

FIG. 2 CURVED DIFFUSER GEOMETRY

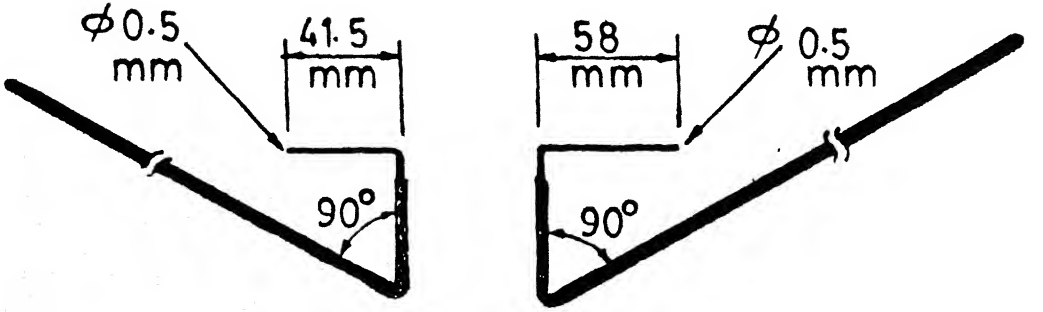

TOTAL HEAD PITOT TUBES FOR INNER & OUTER WALL

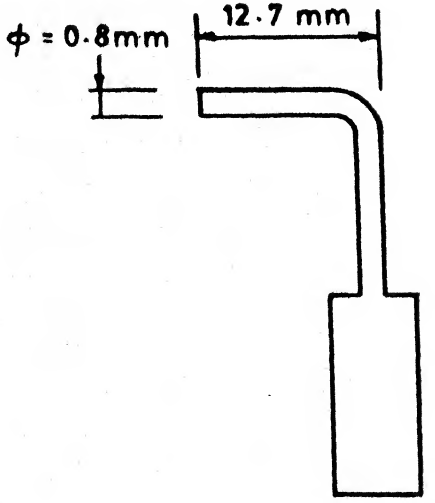

PRESTON TUBE

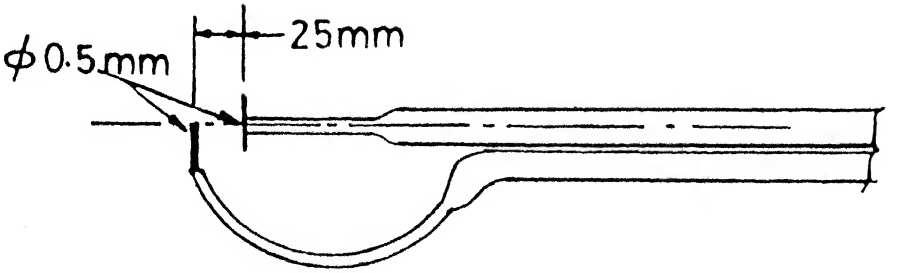

PITOT- DISC PROBE

FIG 3 VARIOUS TYPES OF PROBES

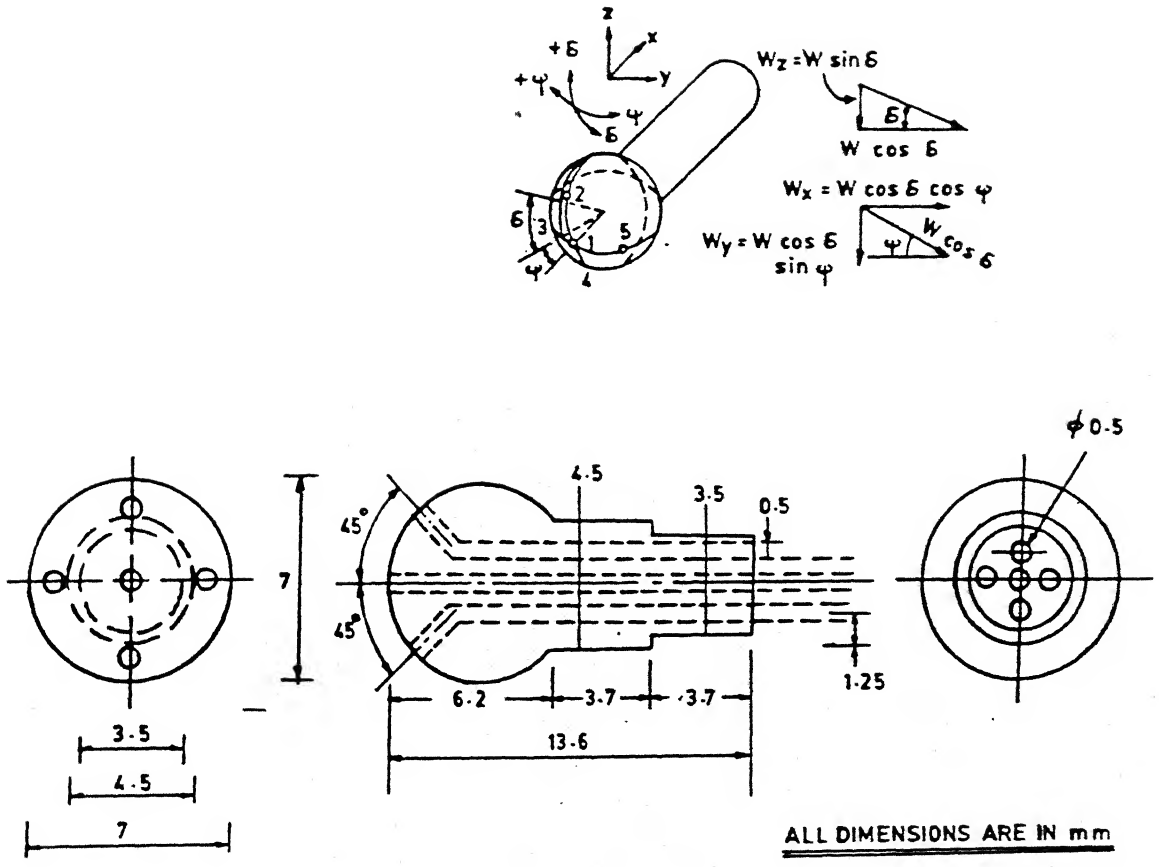

FIG. 4 5 HOLES SPHERICAL PROBE

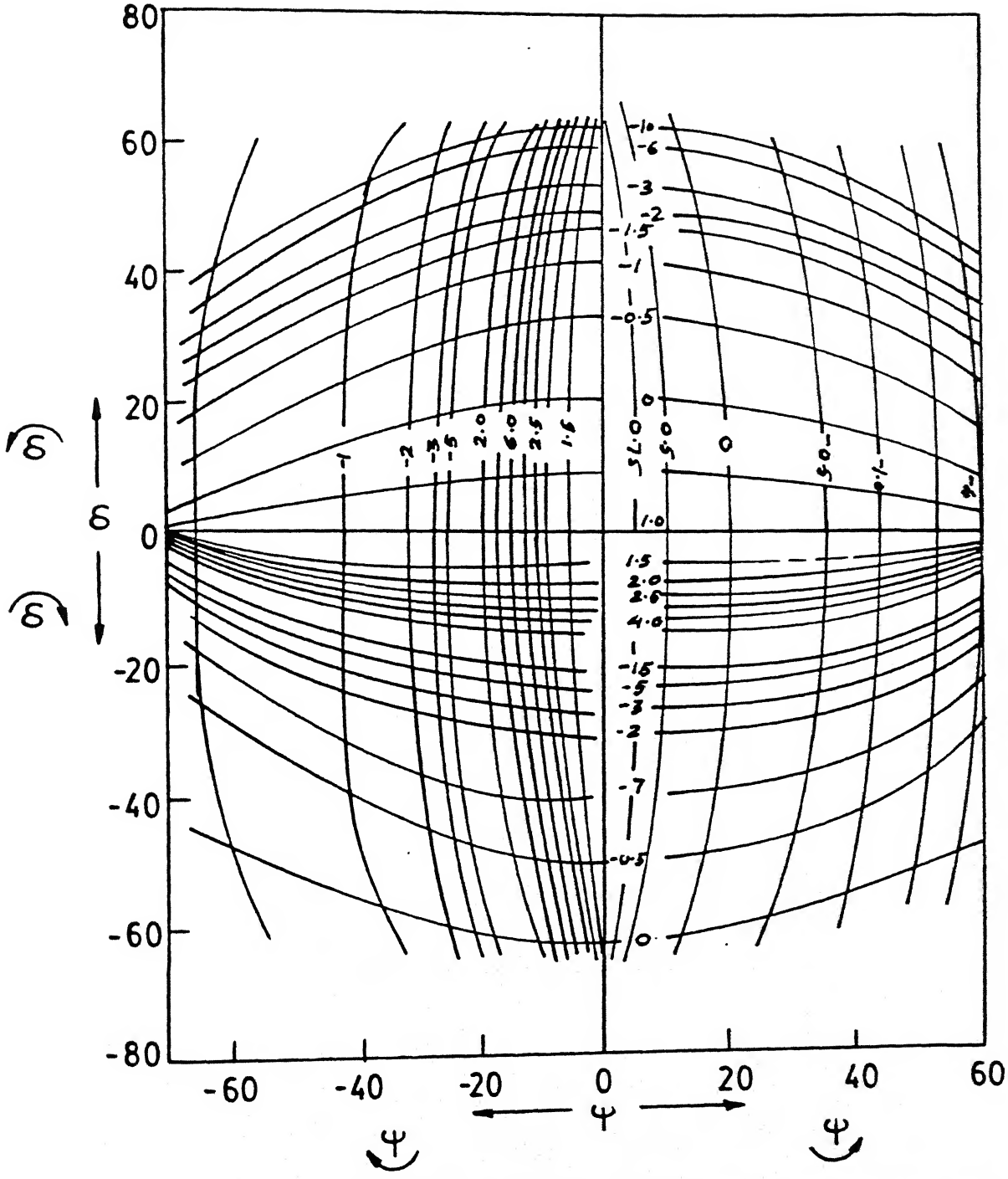

FIG. 5 CALIBRATION CURVES FOR THE INCLINATION FACTORS K_δ & K_ψ

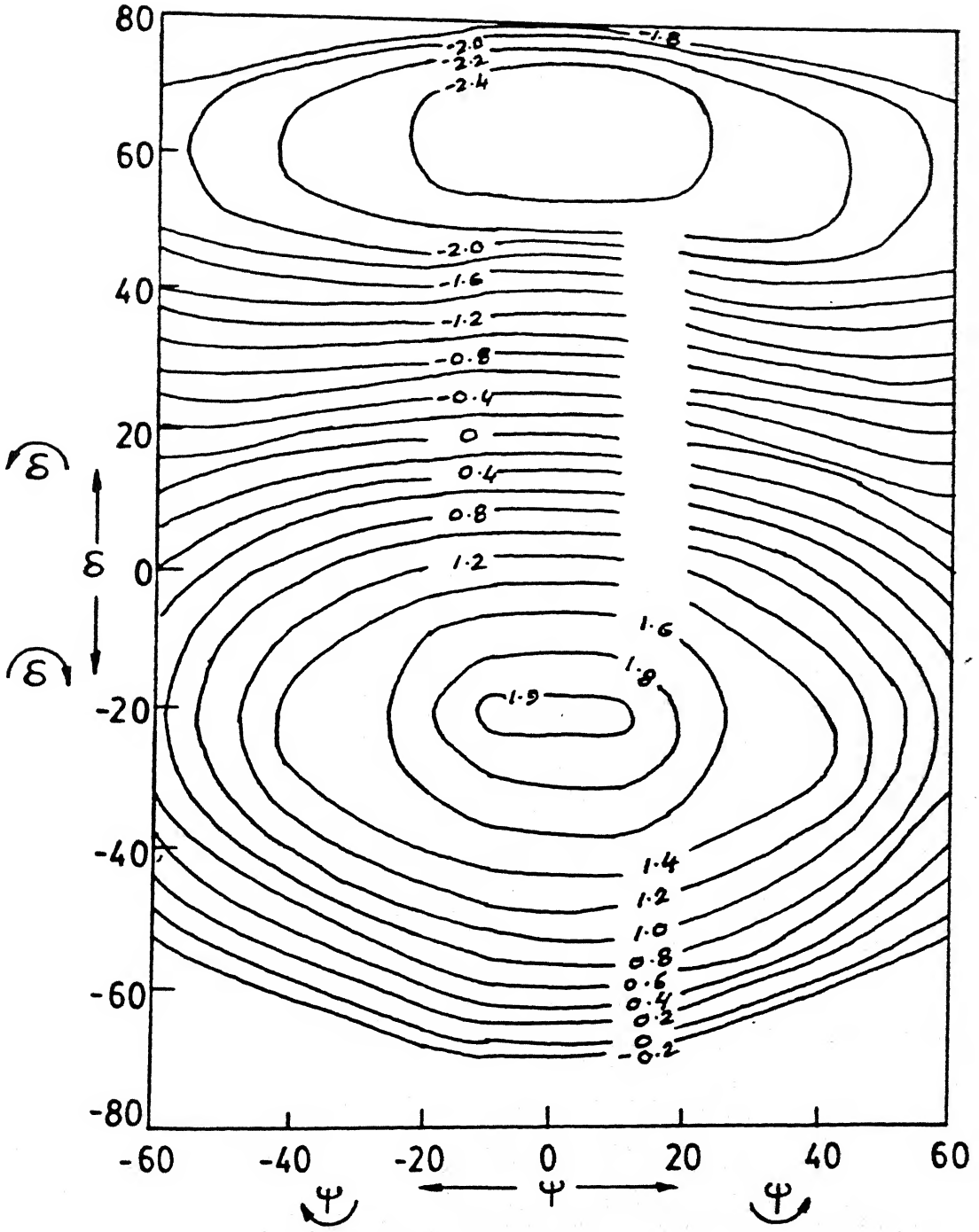

FIG. 6 CALIBRATION CURVES FOR THE VELOCITY FACTOR V_{12}

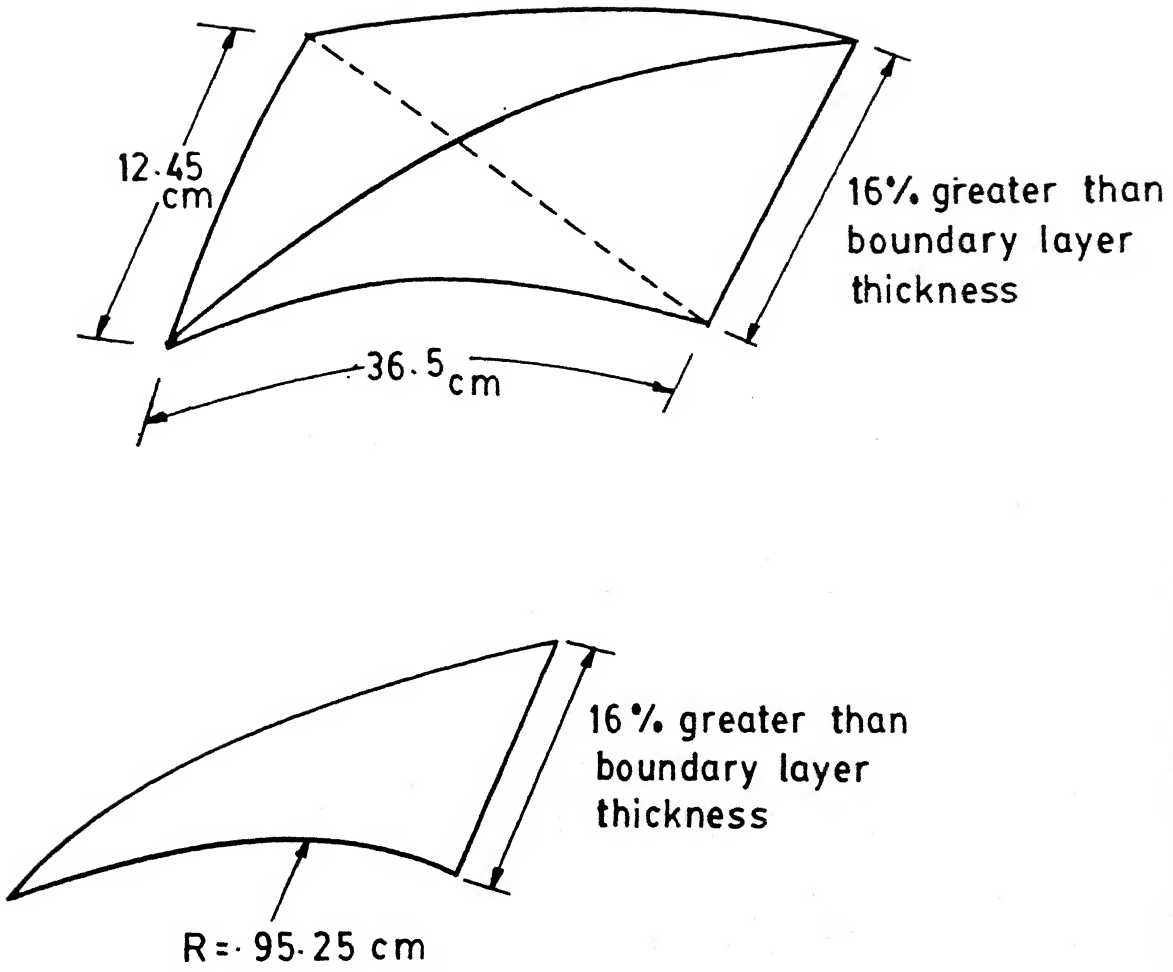

FIG. 7 VORTEX GENERATOR (Curved pyramid)

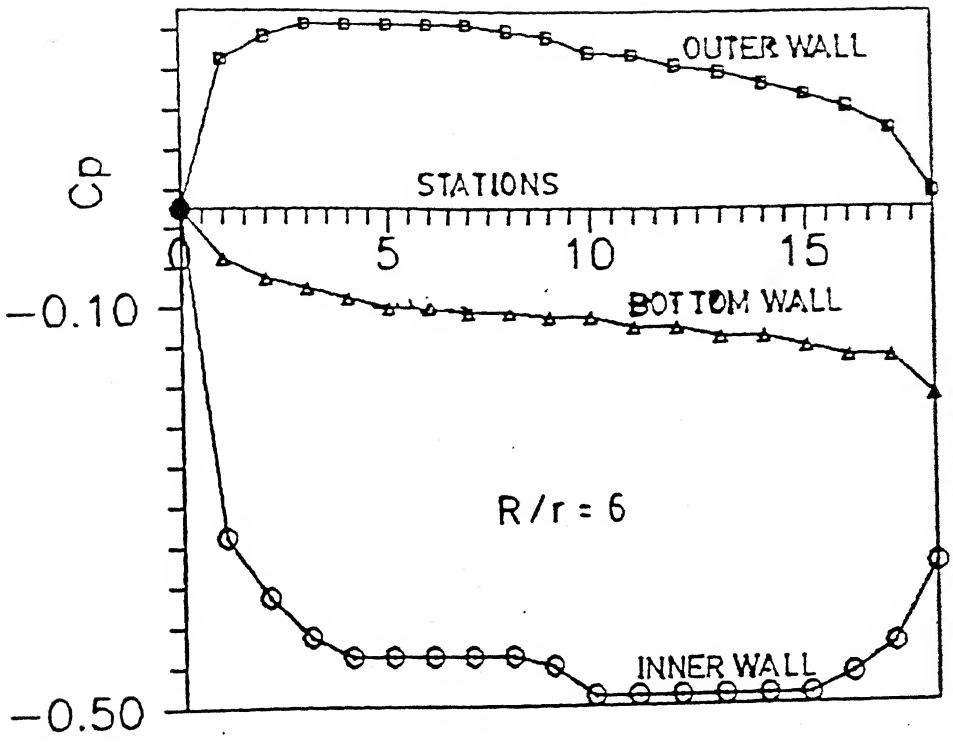

fig. 8 pressure distributions along inner, outer and bottom walls of a curved duct.

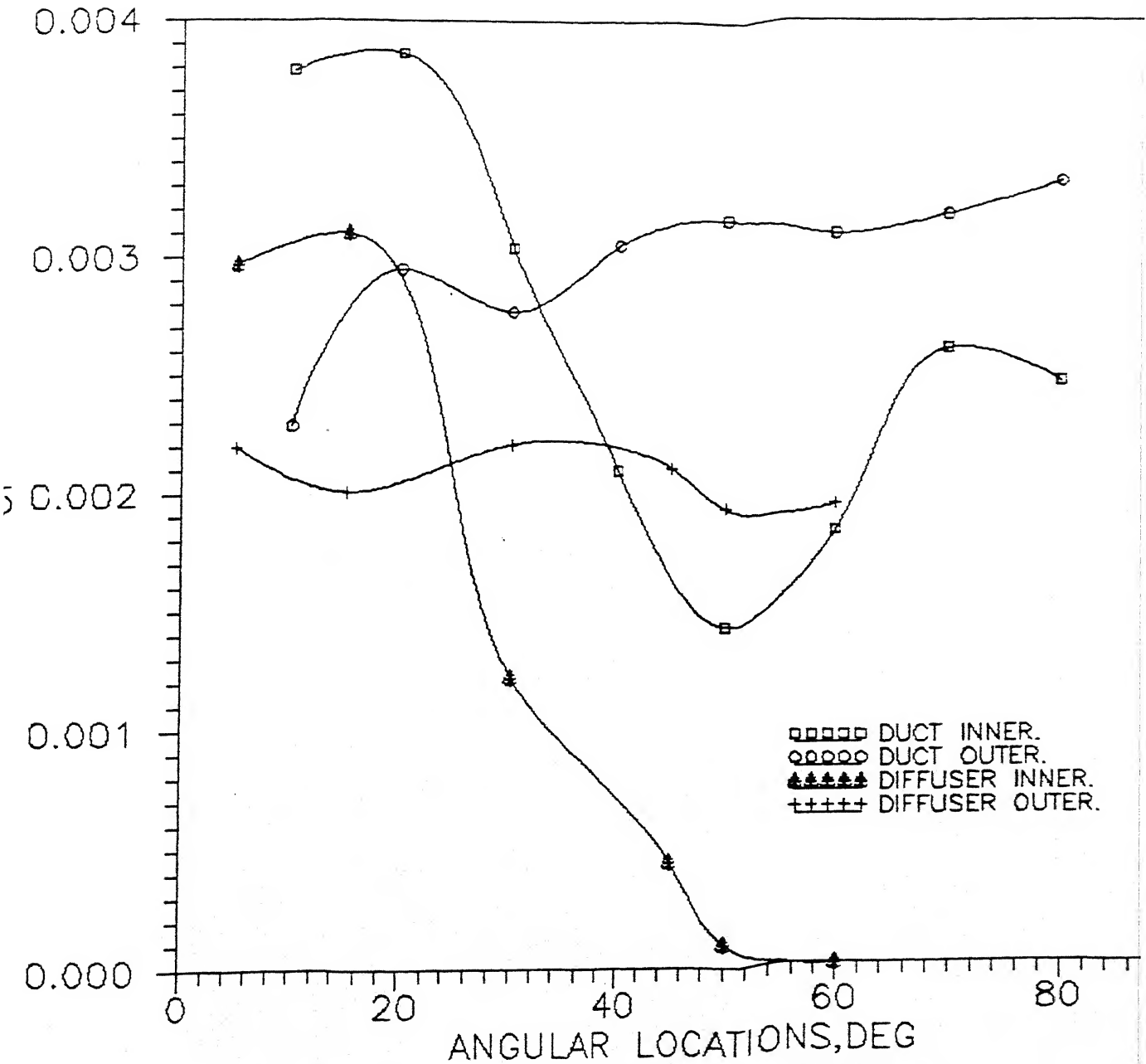

FIG.9 SKIN FRICTION COEFFICIENT DISTRIBUTION IN THF CURVFD DUCT & IN THF 3° DIFFUSFR.

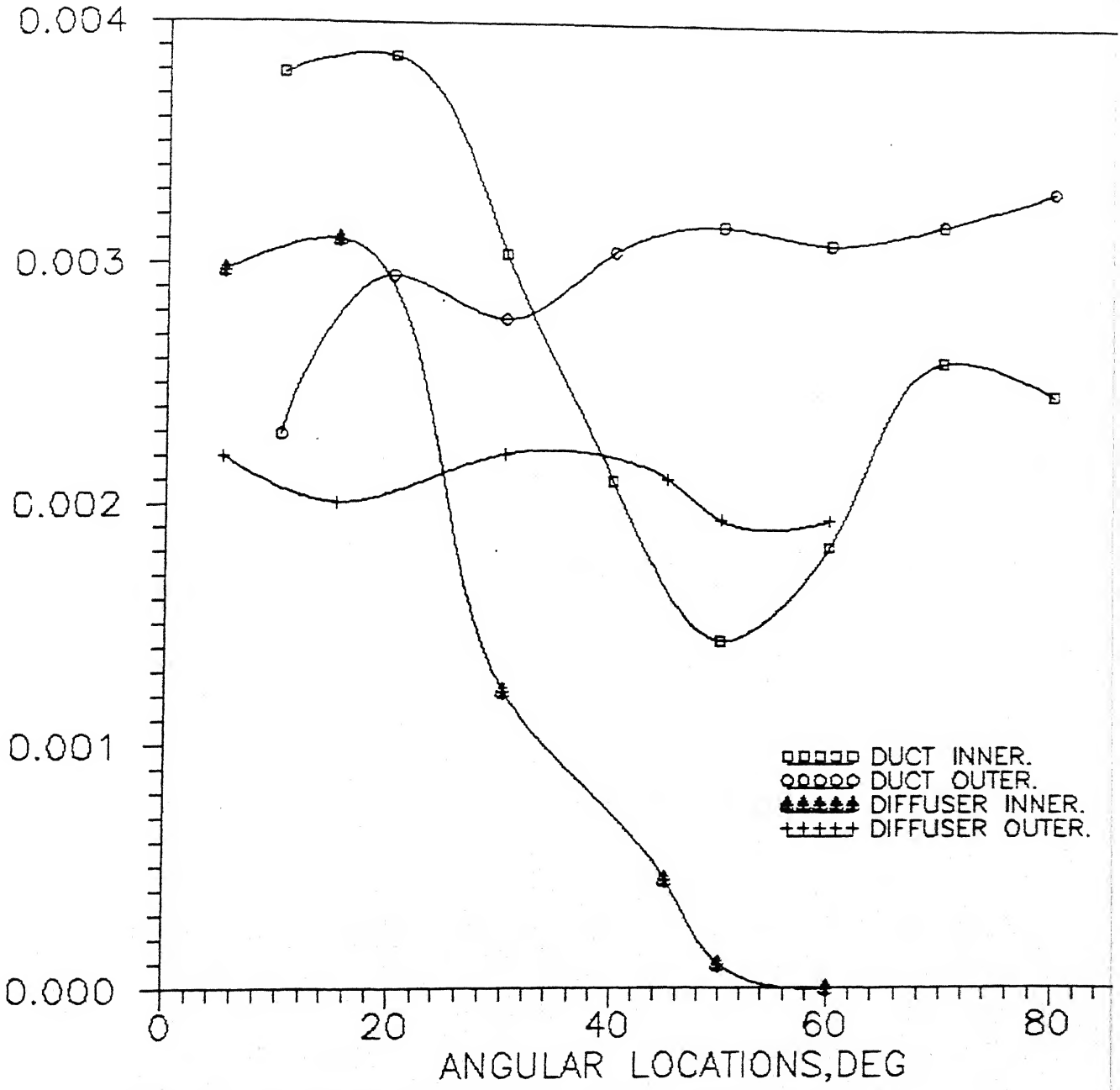

FIG.9 SKIN FRICTION COEFFICIENT DISTRIBUTION IN THF CURVFD DUCT & IN THF 3° DIFFUSFR.

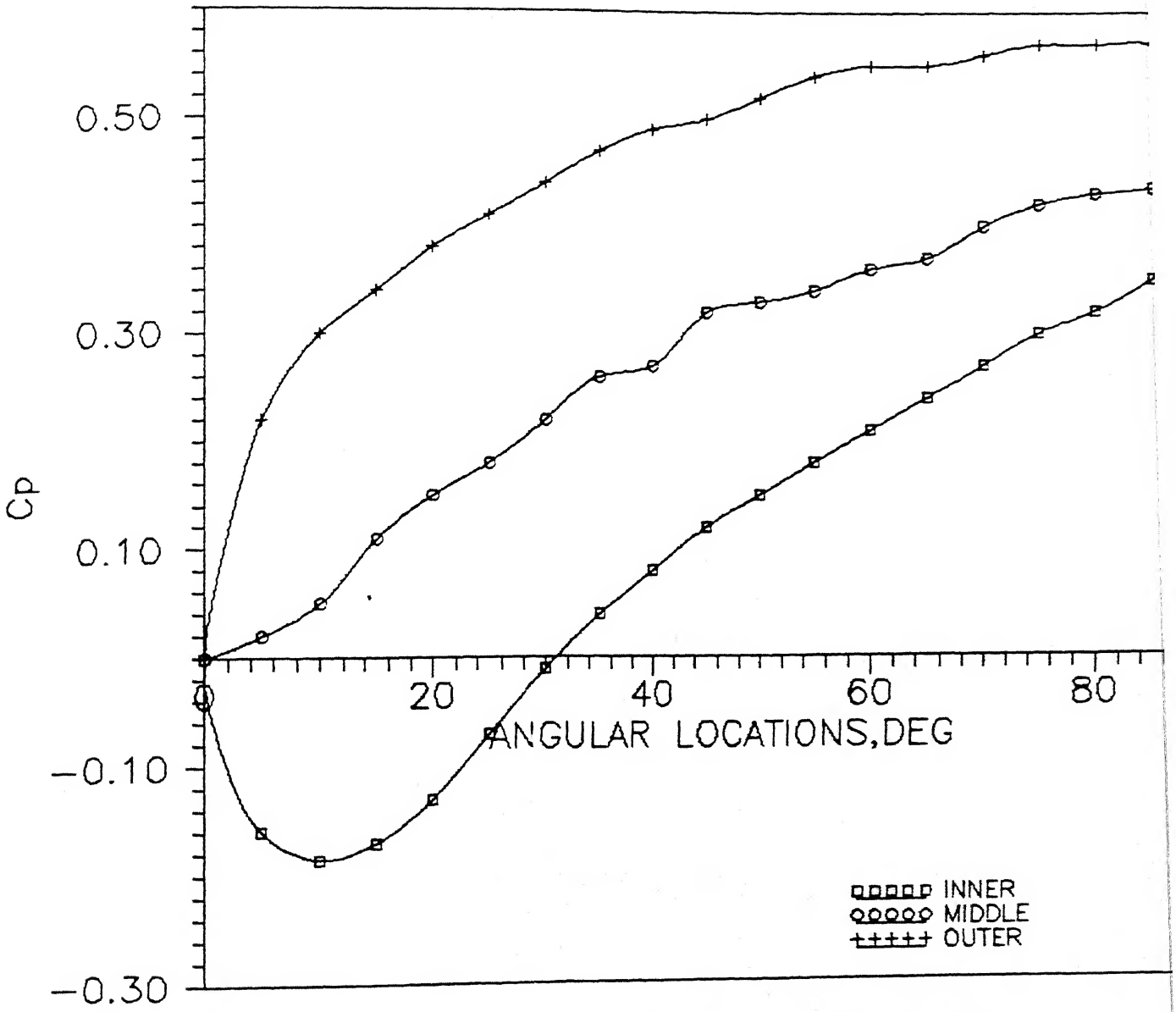

FIG 10 STATIC PRESSURE EFFICIENT DISTRIBUTION IN THE 3° DIFFUSER.

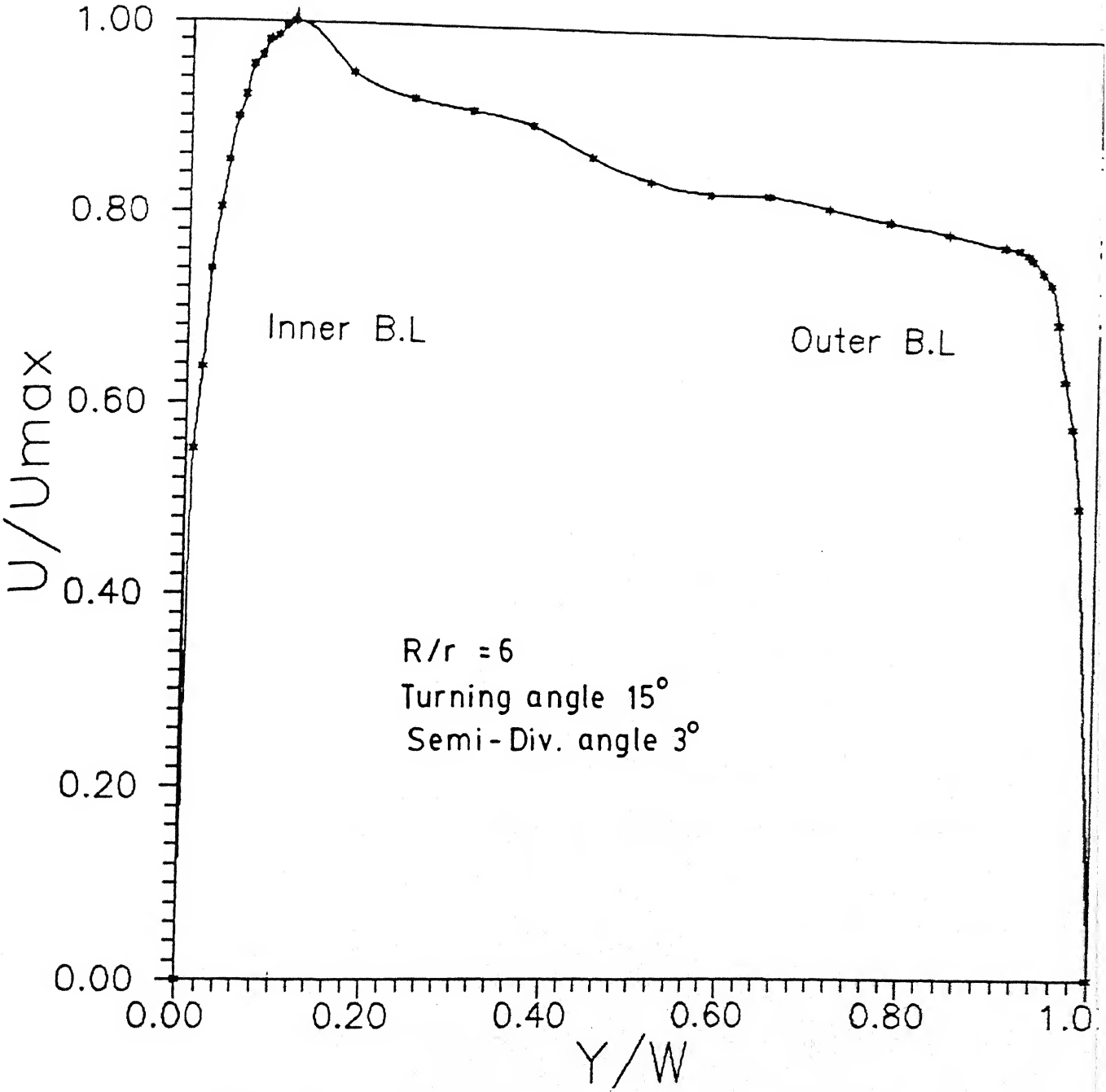

FIG. 11 VELOCITY DISTRIBUTION (Radial)

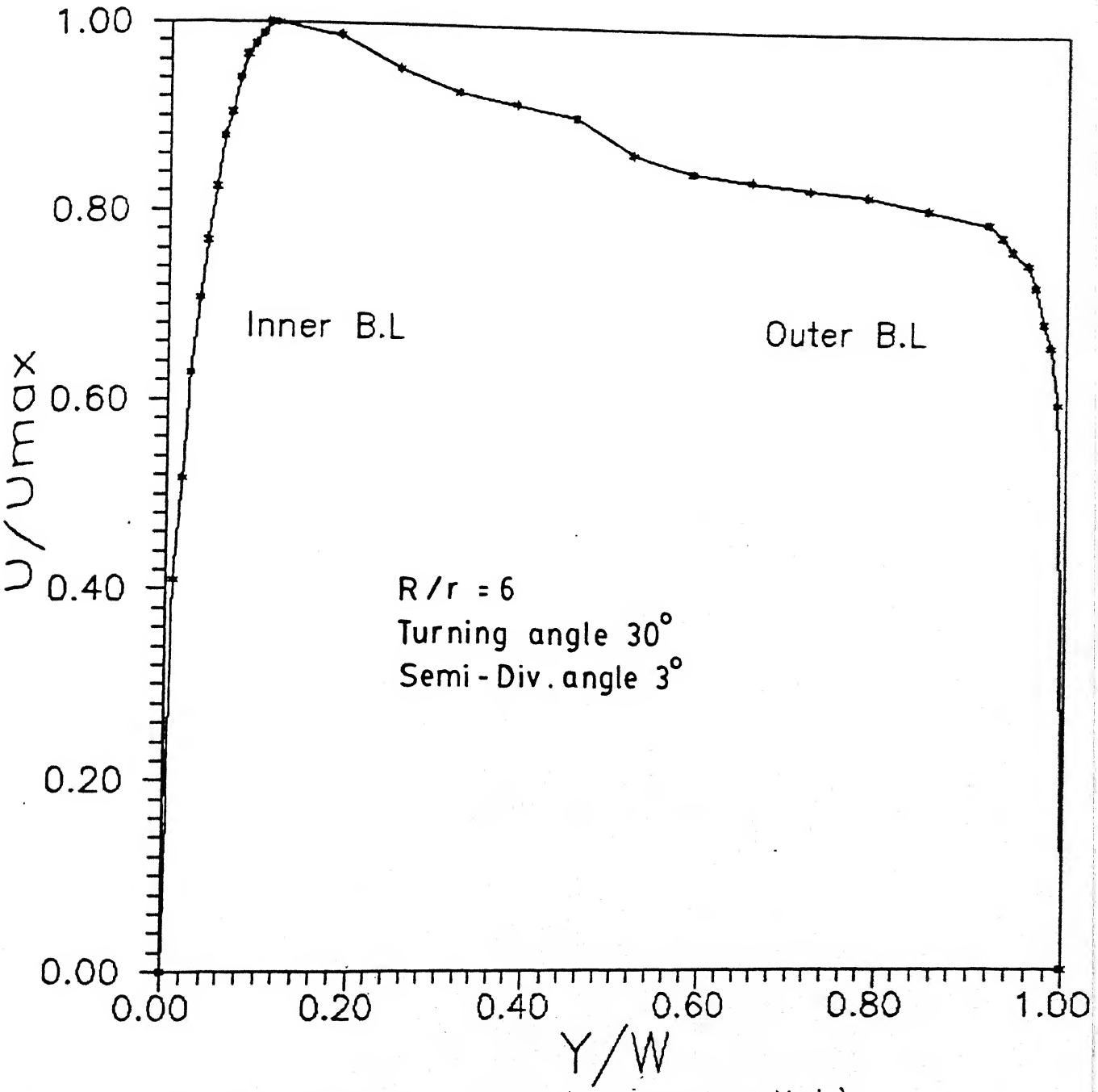

FIG. 12 VELOCITY DISTRIBUTION (Radial)

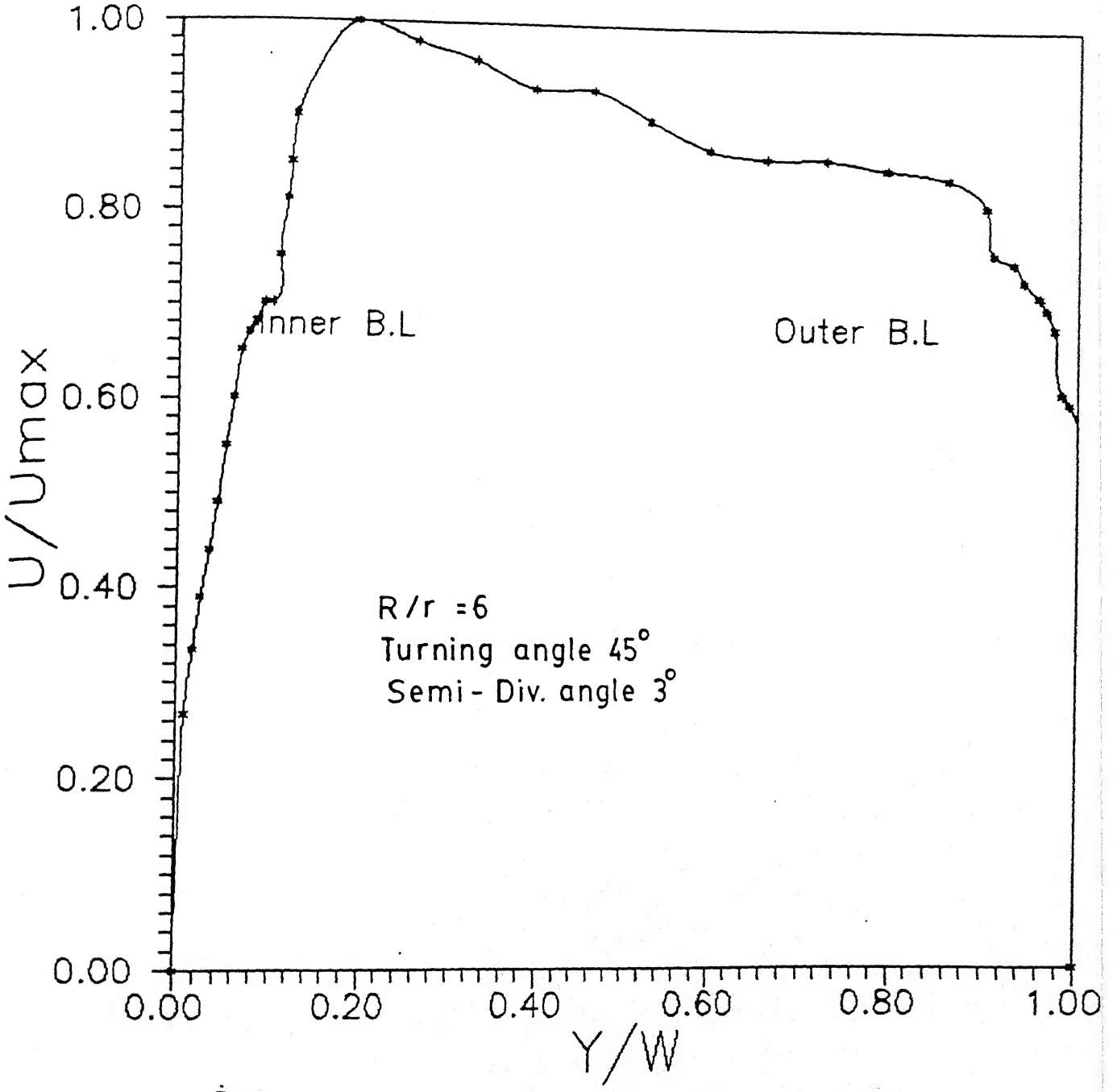

FIG. 13 VELOCITY DISTRIBUTION (Radial)

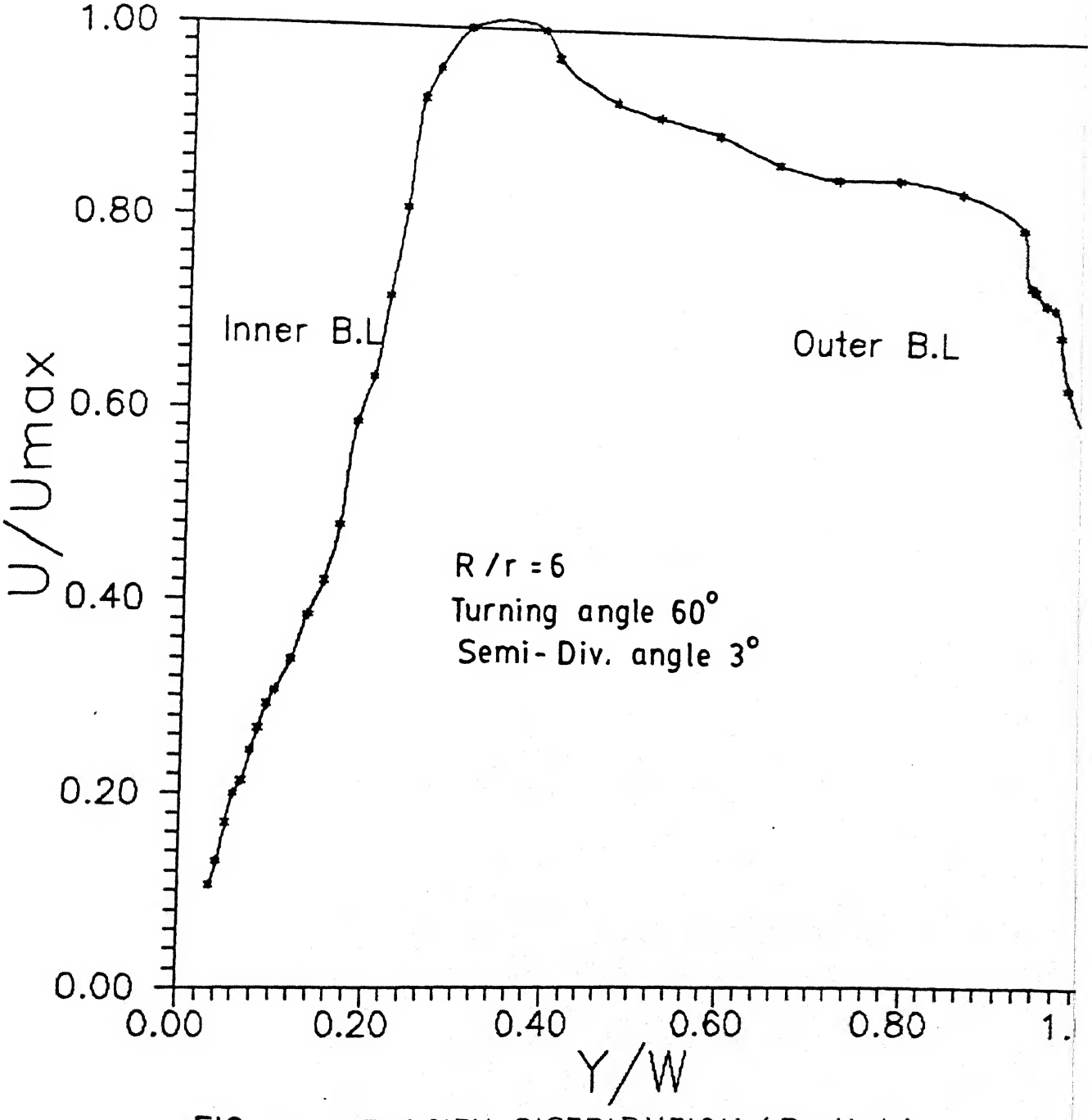

FIG. 14 VELOCITY DISTRIBUTION (Radial)

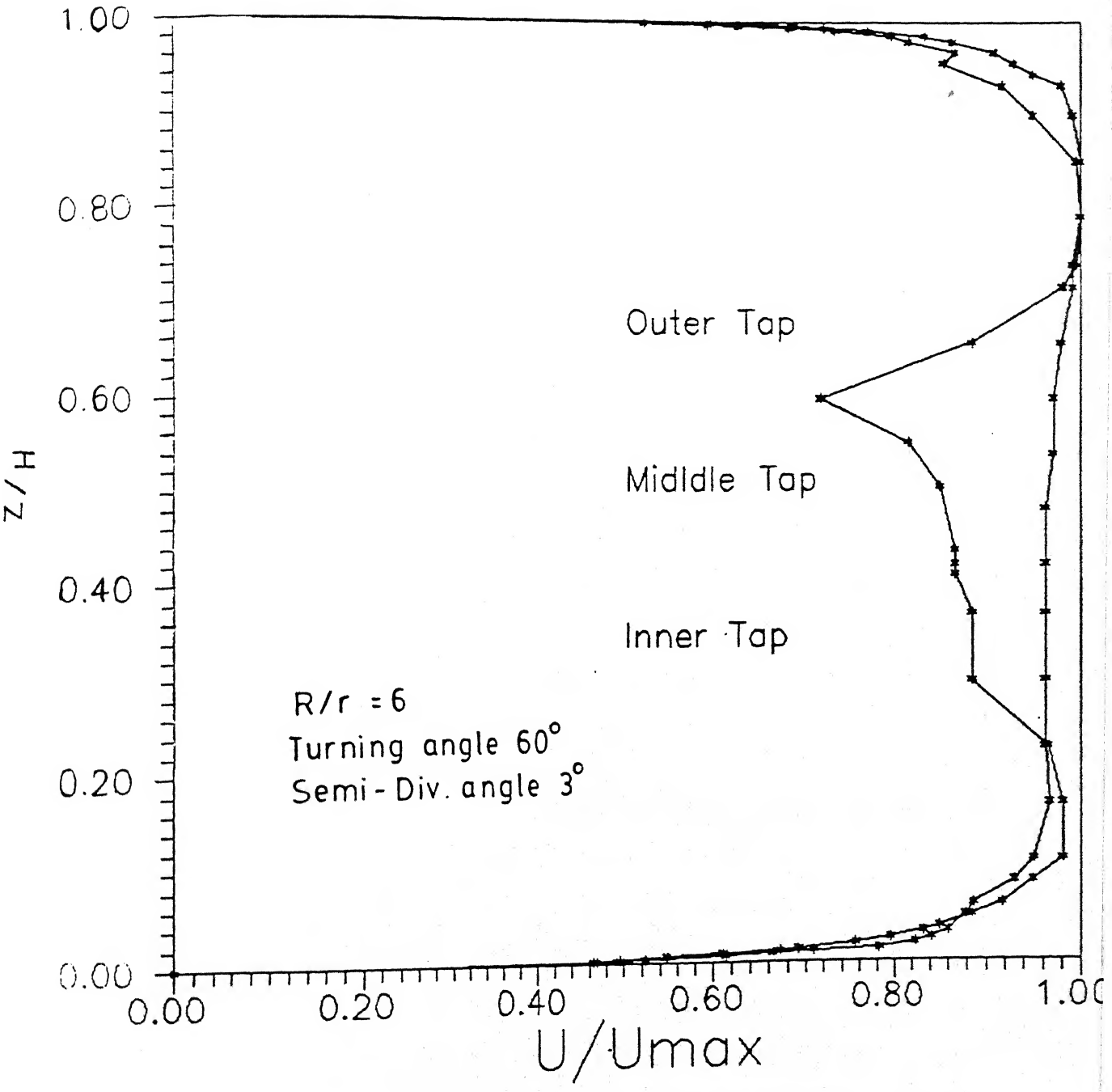

FIG. 15 VELOCITY DISTRIBUTION (Spanwise)

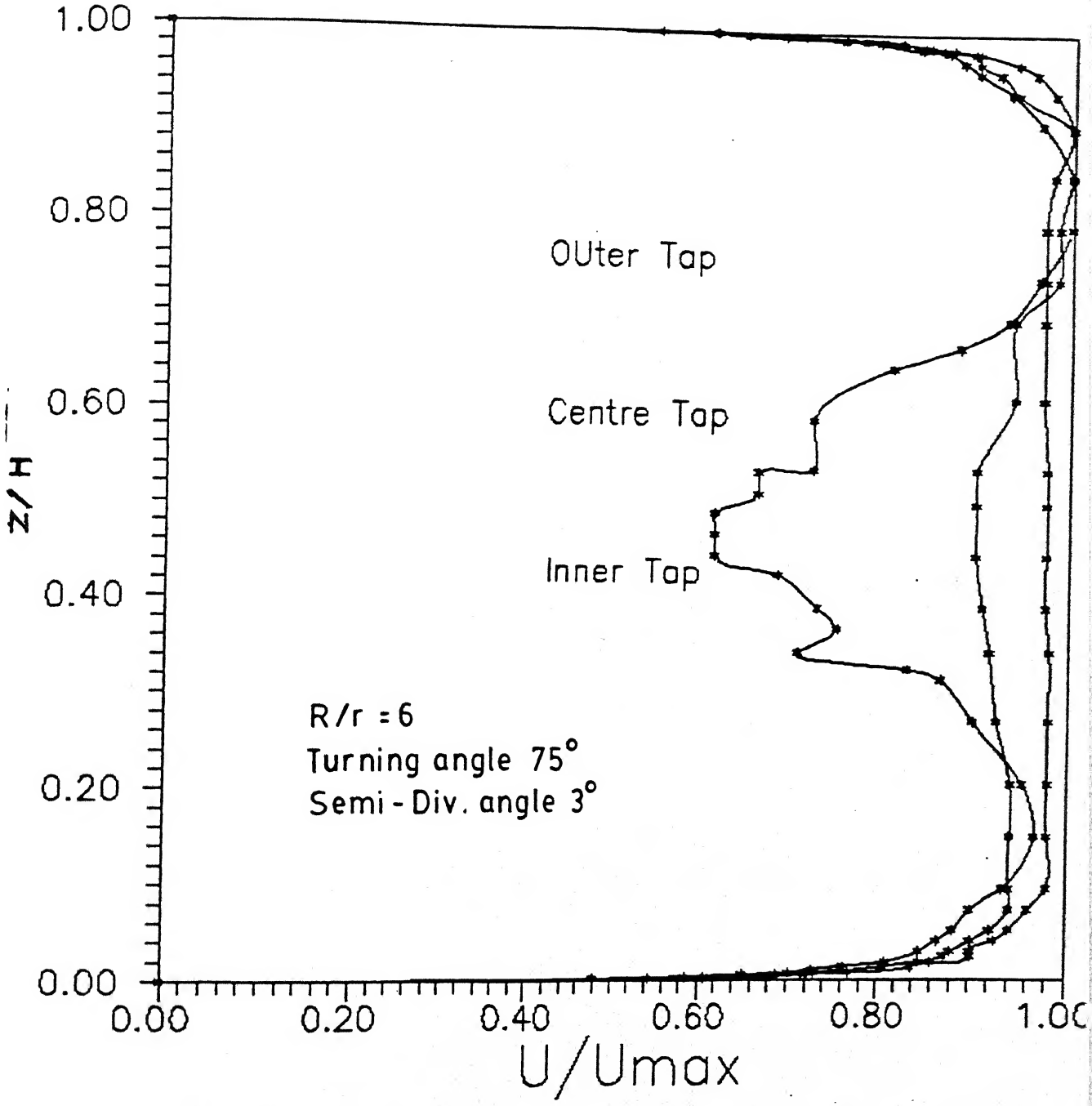

FIG. 16 VELOCITY DISTRIBUTION (Spanwise)

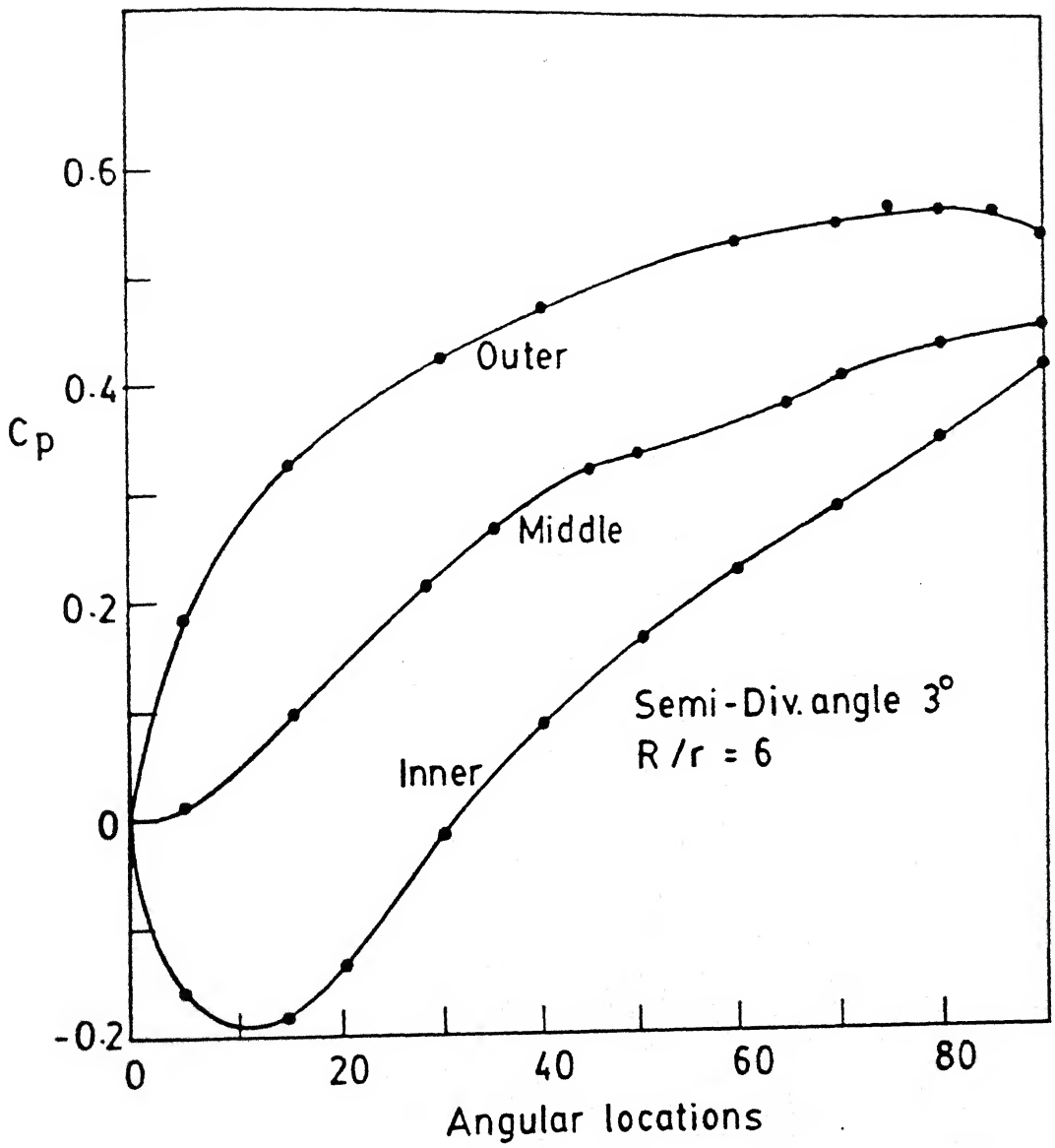

FIG. 17 STATIC PRESSURE COEFFICIENT DISTRIBUTION WITH GRID

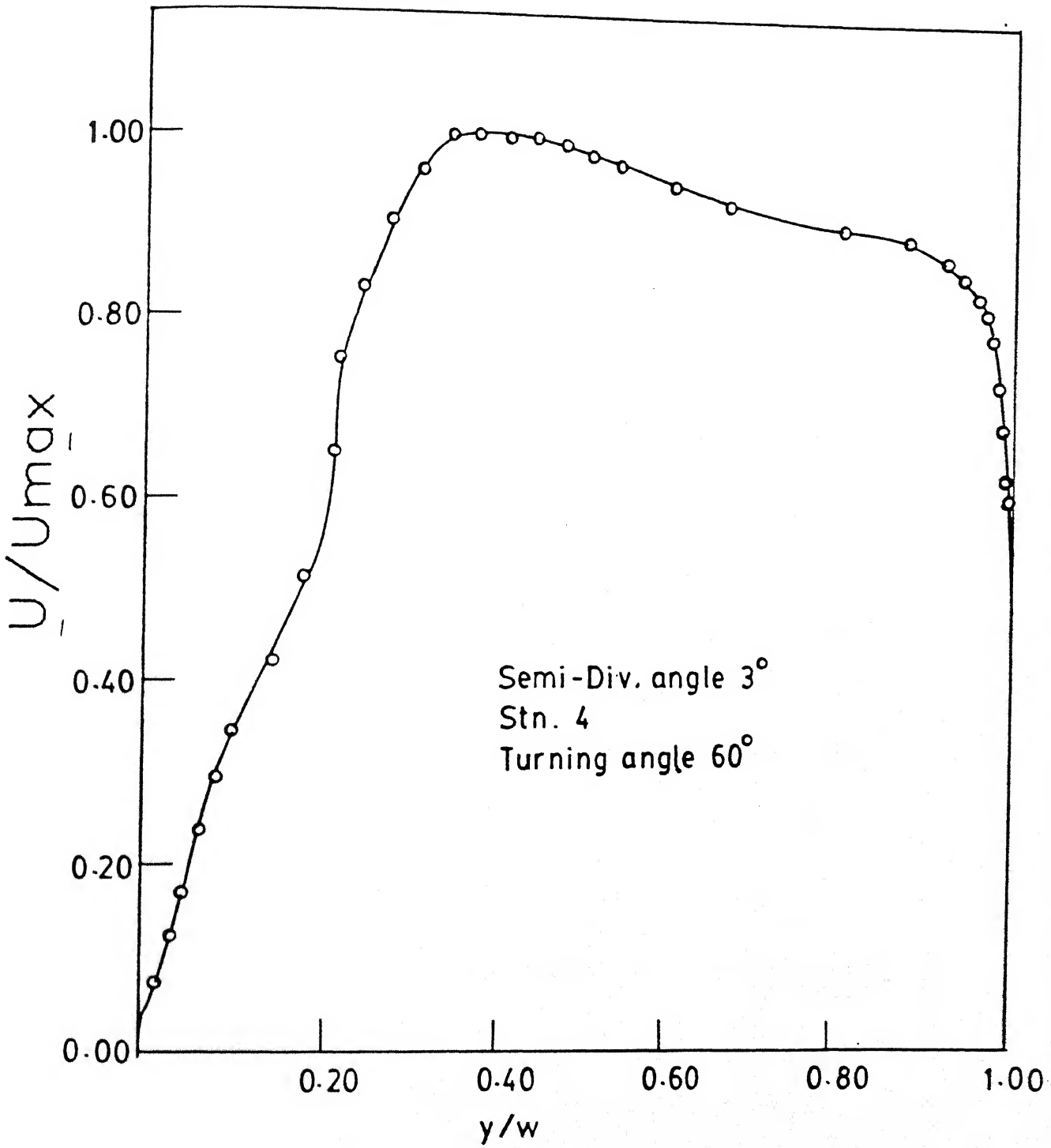

FIG. 18 VELOCITY DISTRIBUTION (Radial) WITH GRID

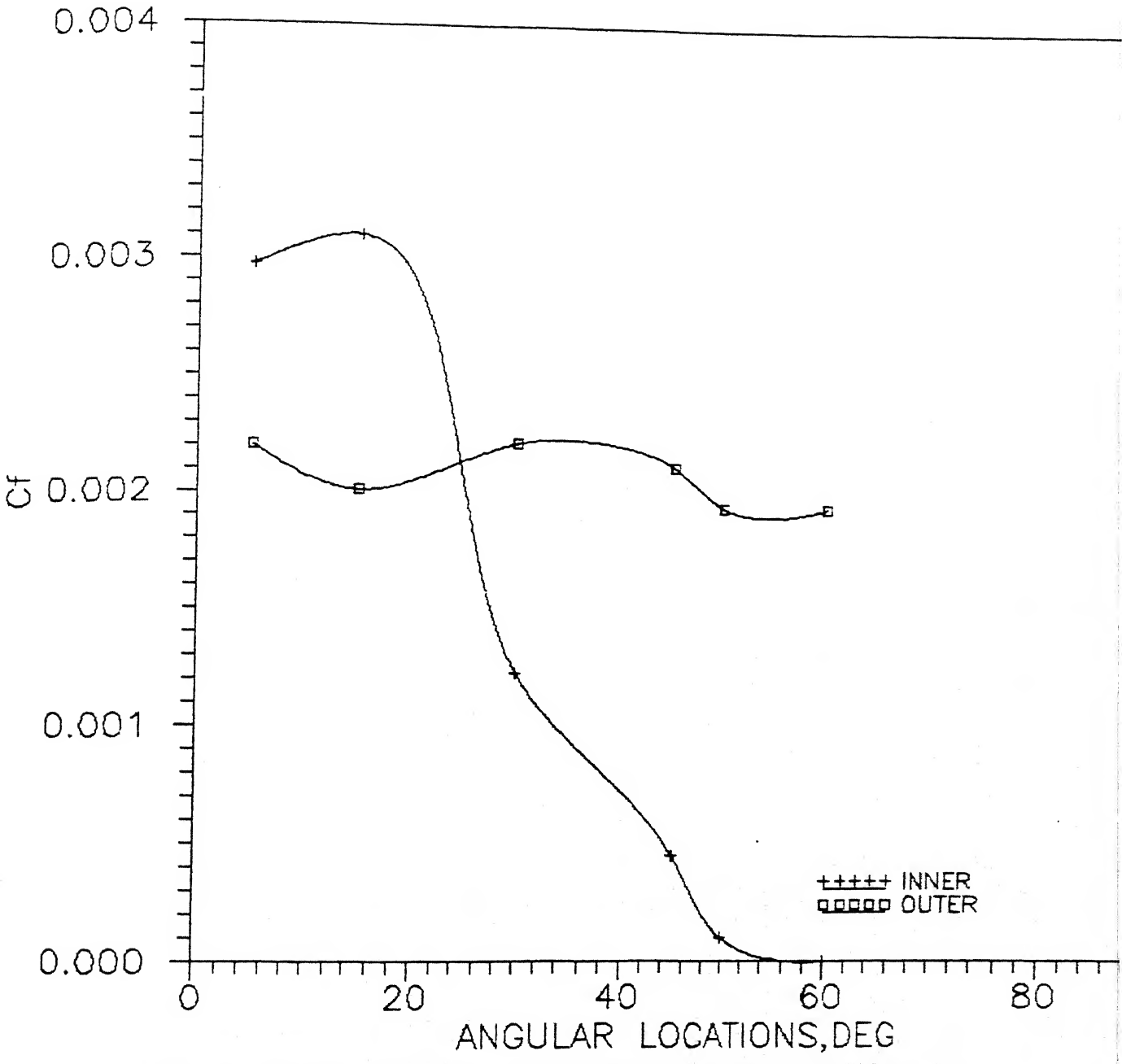

FIG.19 SKIN FRICTION COEFFICIENT DISTRIBUTION IN THF 3° DIFFUSFR.

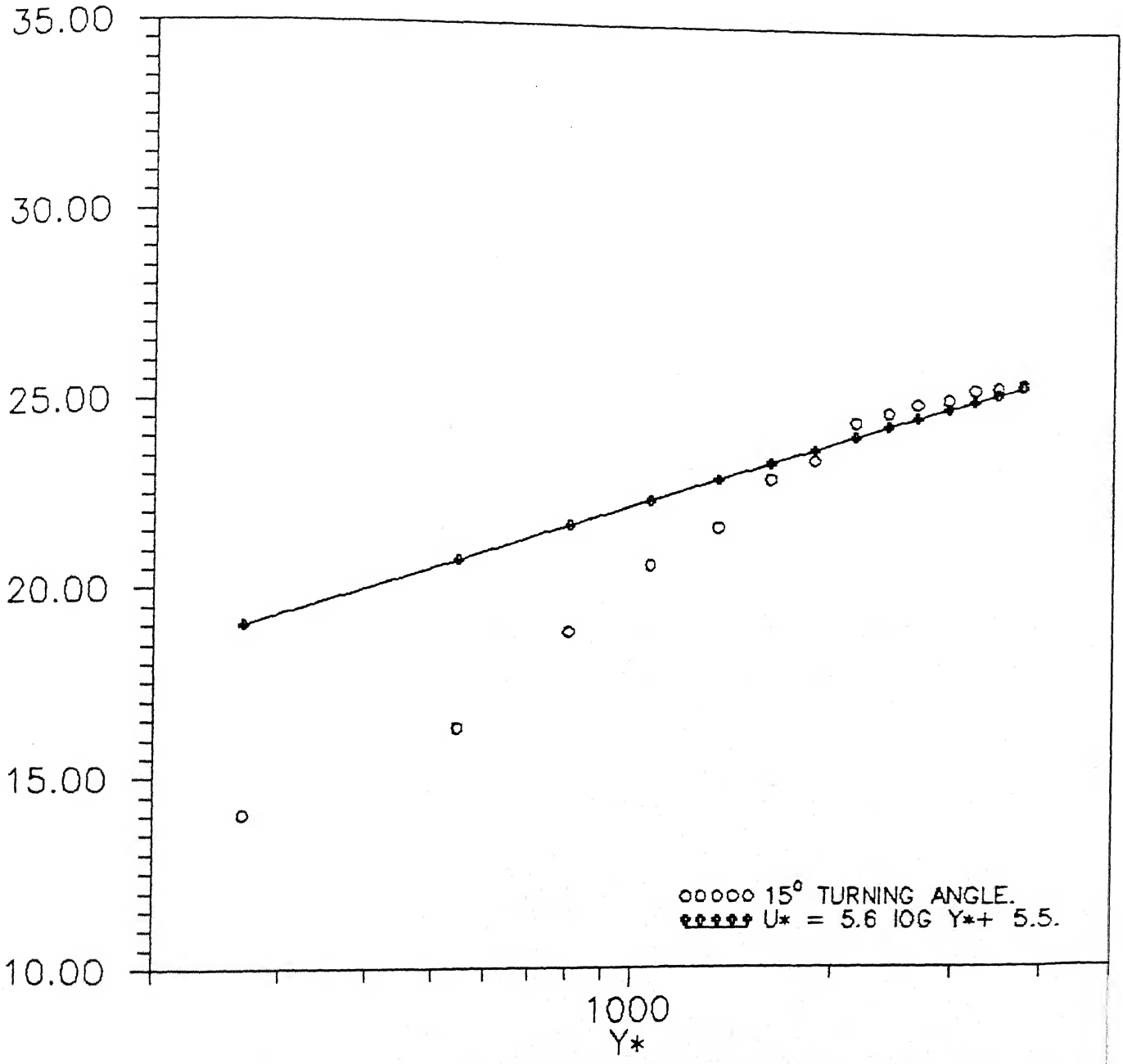

FIG.20 MEAN VELOCITY DISTRIBUTION ACROSS THE INNER WALL BOUNDARY LAYER (3° DIFFUSER).

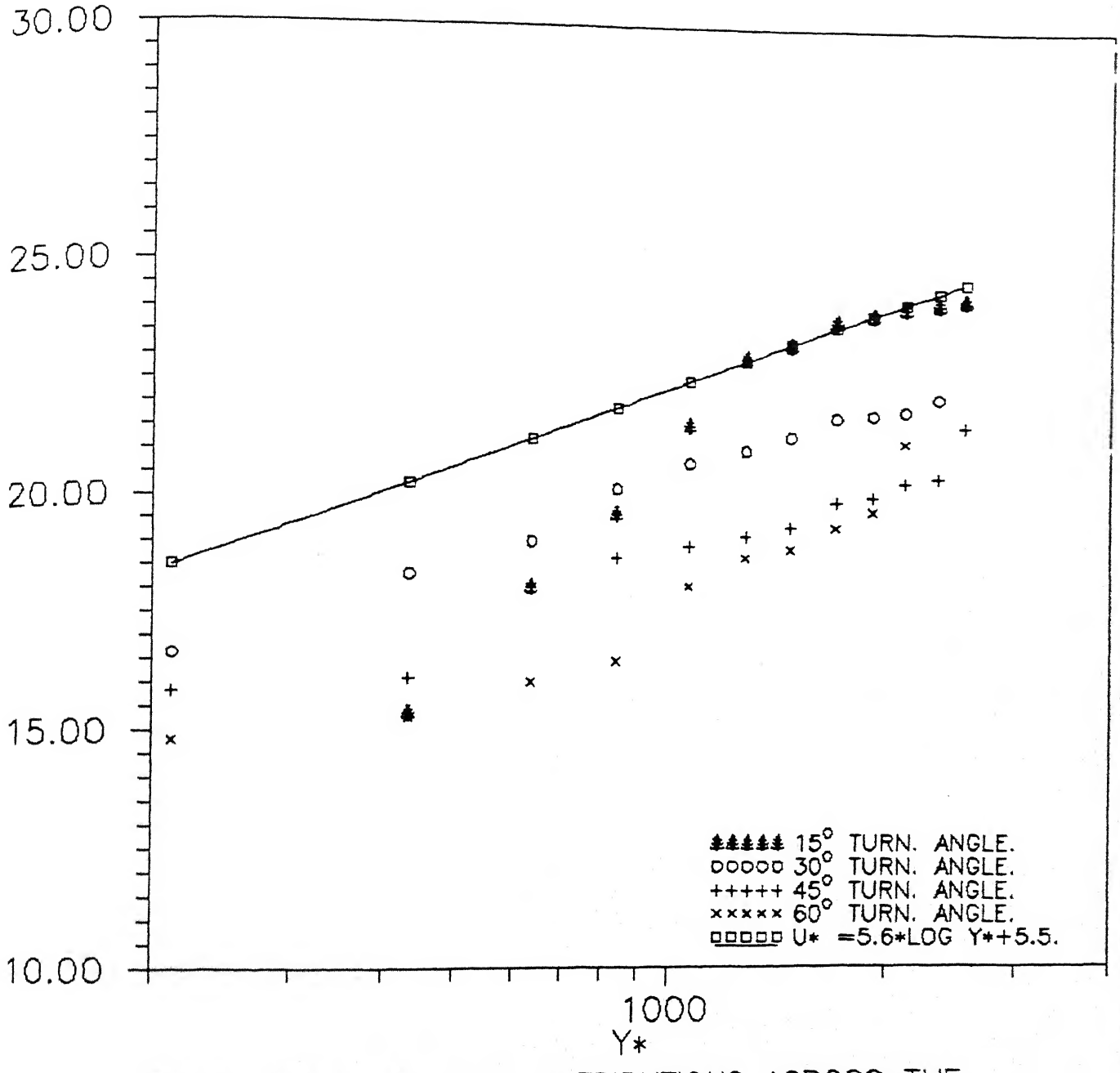

FIG.21 MEAN VELOCITY DISTRIBUTIONS ACROSS THE OUTER WALL BOUNDARY LAYER (3° DIFFUSER).

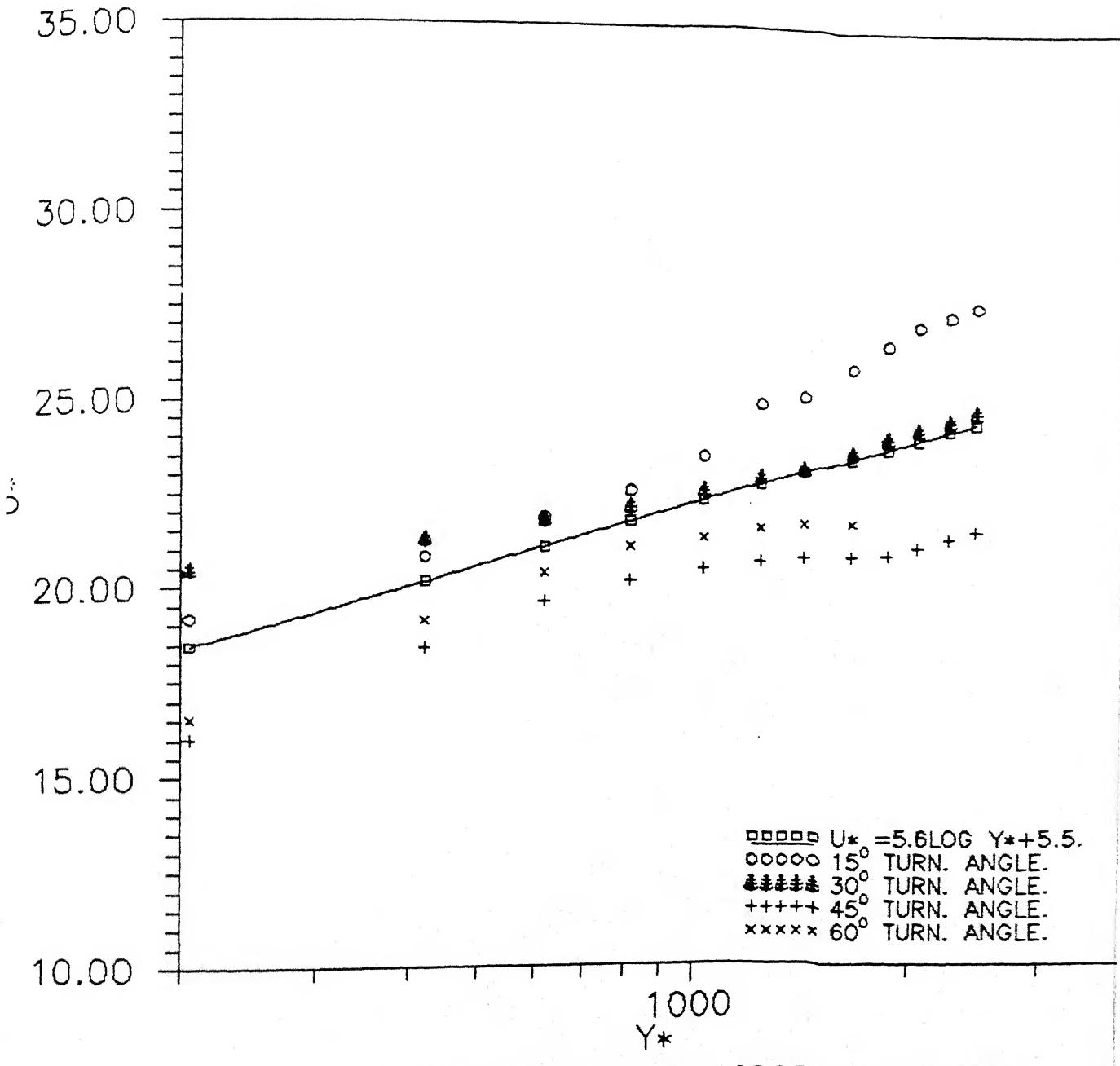

FIG.22 MEAN VELOCITY DISTRIBUTIONS ACROSS THE OUTER WALL BOUNDARY LAYER WITH GRID (3° DIFFUSER).

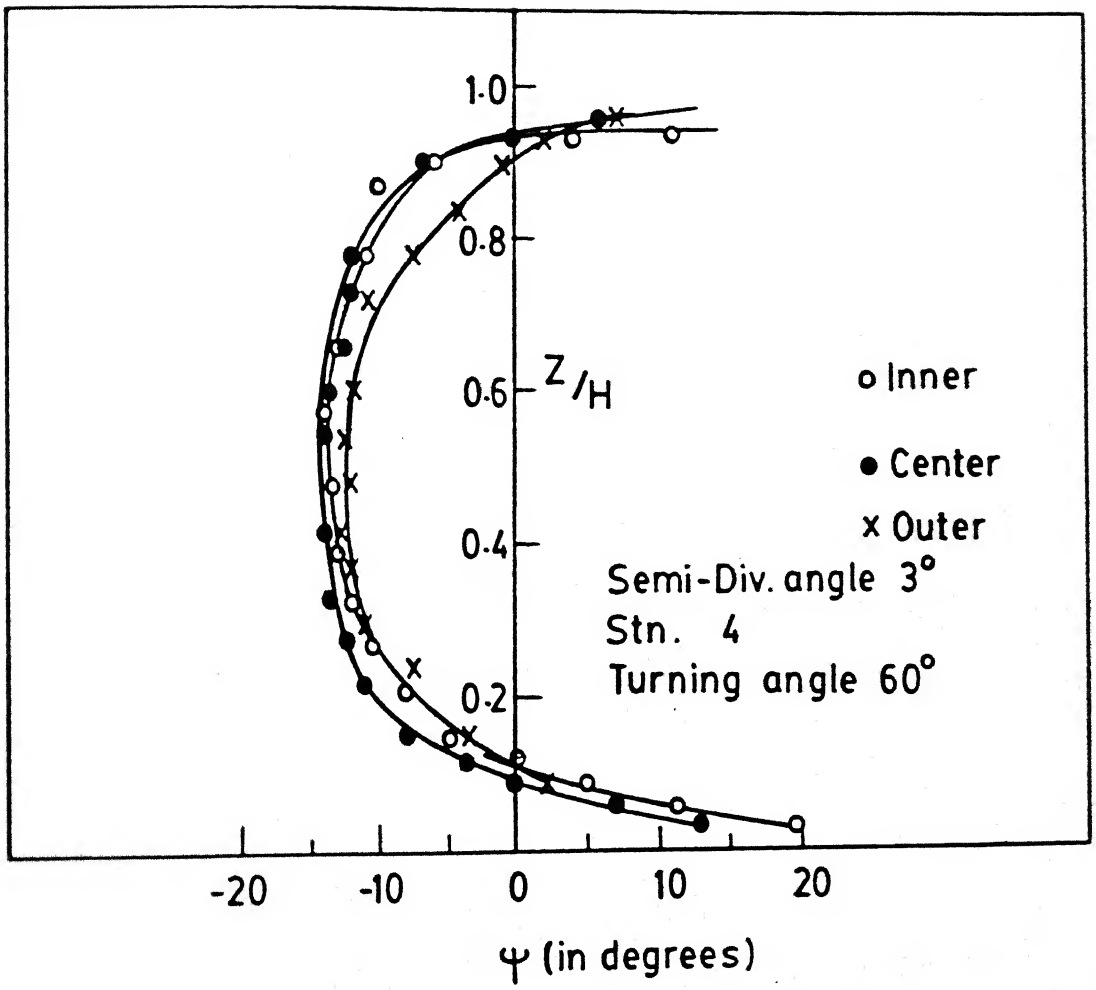

FIG. 23 FLOW ANGLE DISTRIBUTION

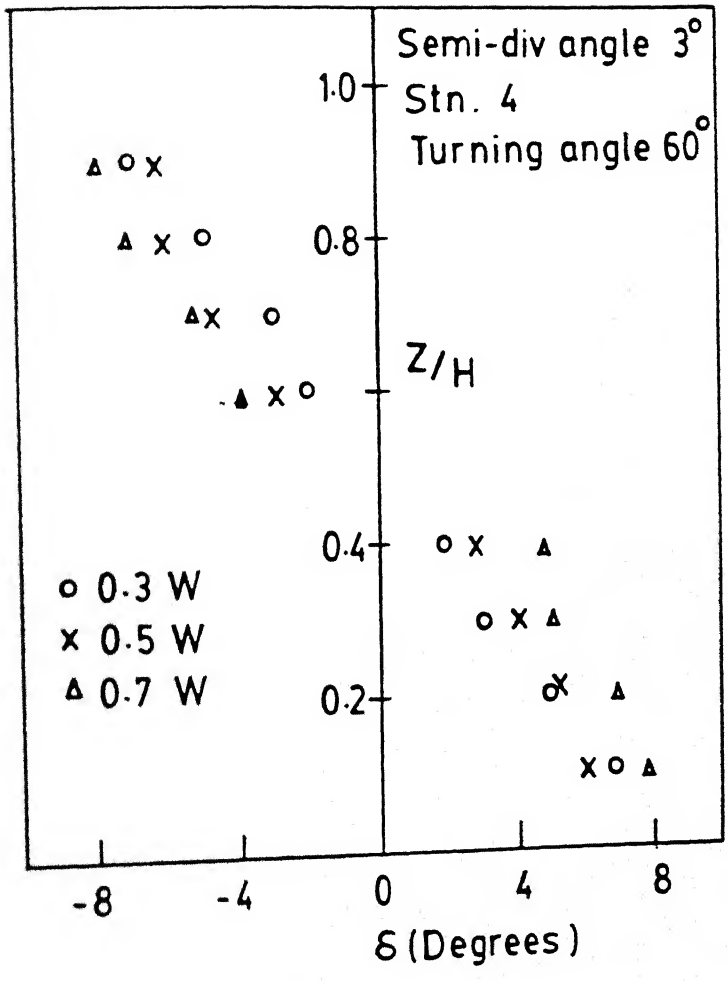

FIG. 24 SPANWISE VARIATION OF PITCH ANGLE

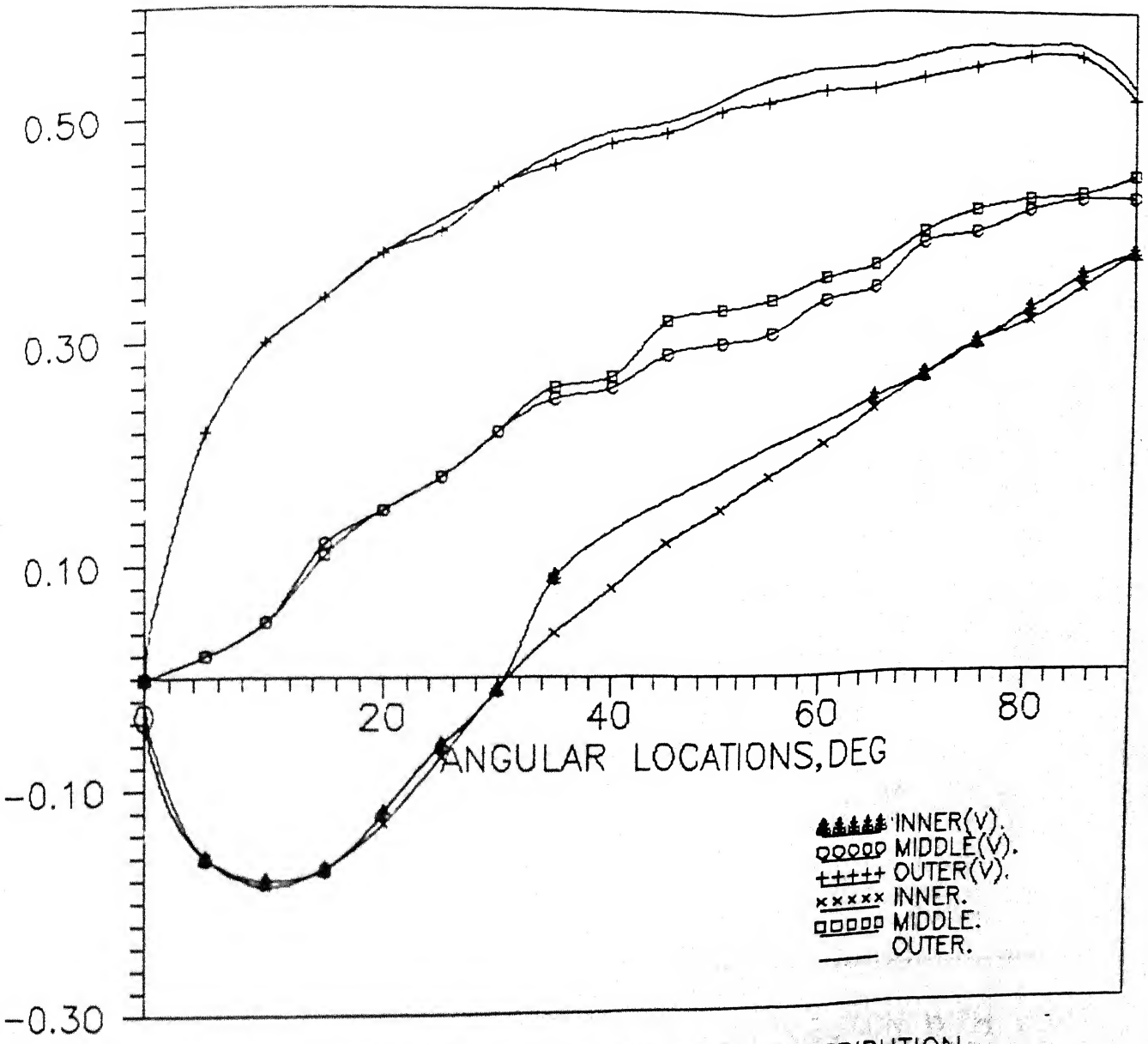

FIG.25 STATIC PRESSURE COEFFICIENT DISTRIBUTION WITH VORTEX GENERATOR(16%) FROM 38° TO 60°.

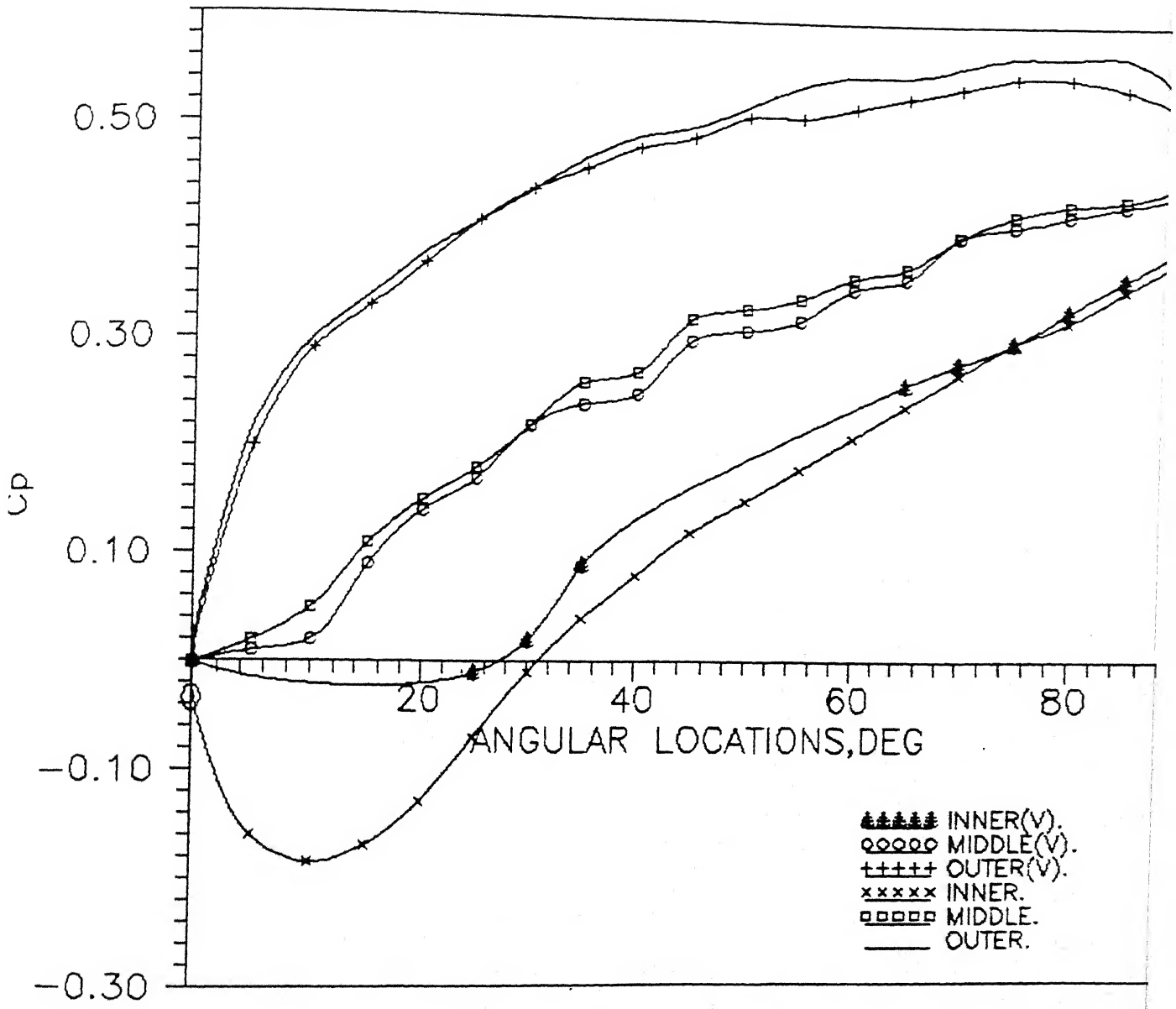

FIG.26 STATIC PRESSURE COEFFICIENT DISTRIBUTION WITH VORTI
GENERATOR(1.6%) FROM 0^0 TO 20^0 & FROM 38^0 TO 6

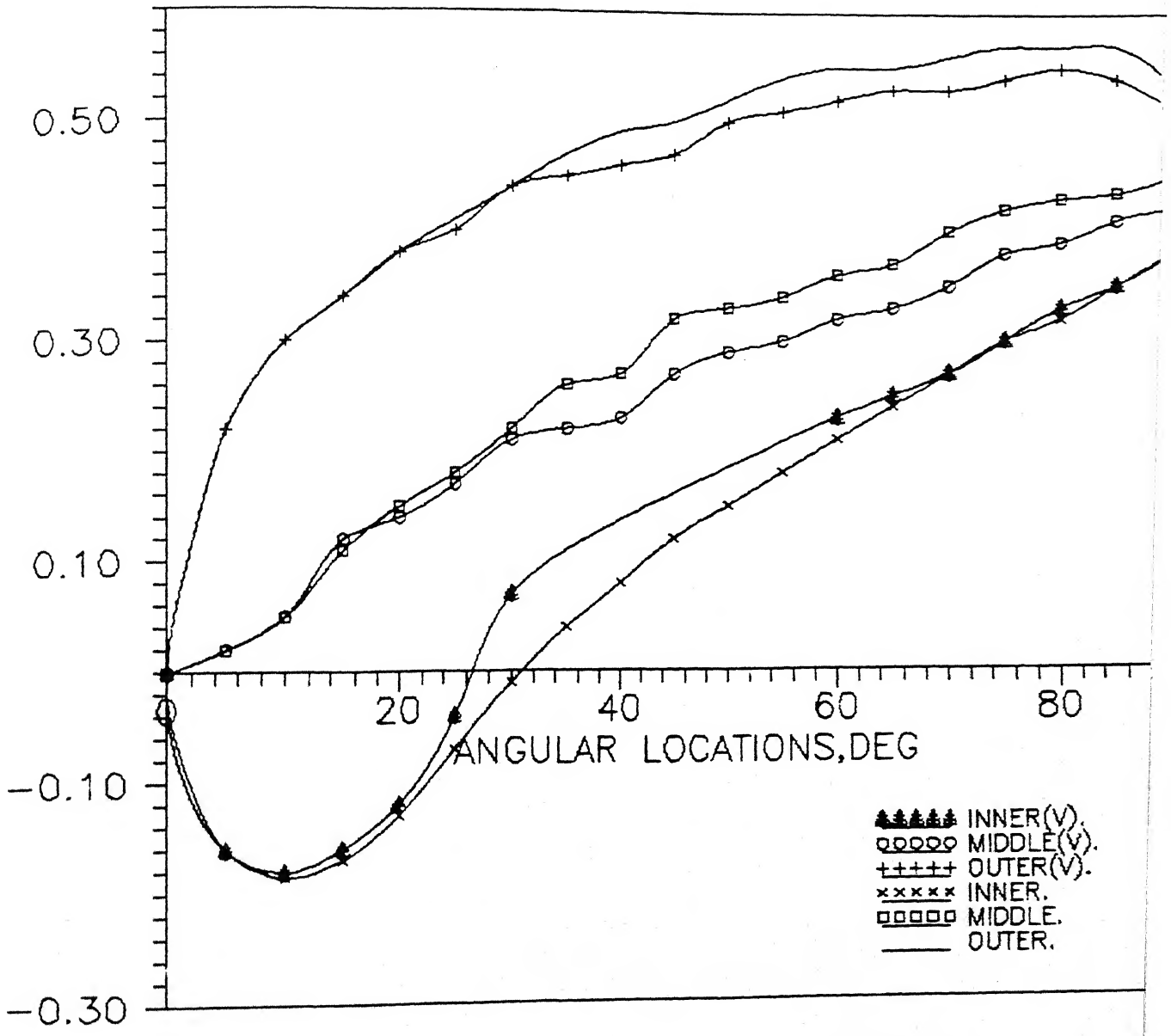

FIG.27 STATIC PRESSURE COEFFICIENT DISTRIBUTION WITH VORTEX GENERATOR(18%) FROM 33° TO 55°.

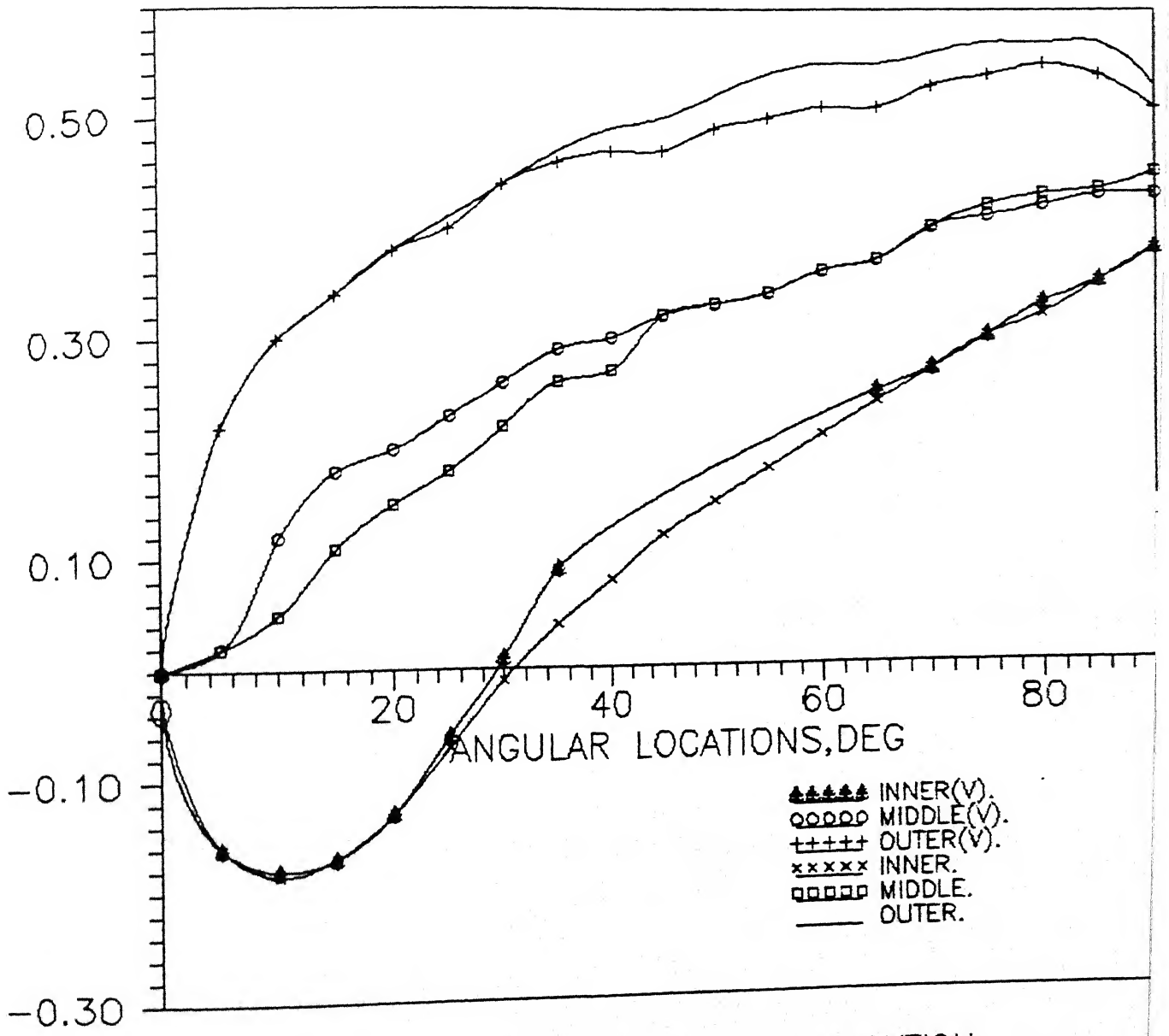

FIG.28 STATIC PRESSURE COEFFICIENT DISTRIBUTION WITH VORTEX GENERATOR(11%) FROM 38° TO 60°.

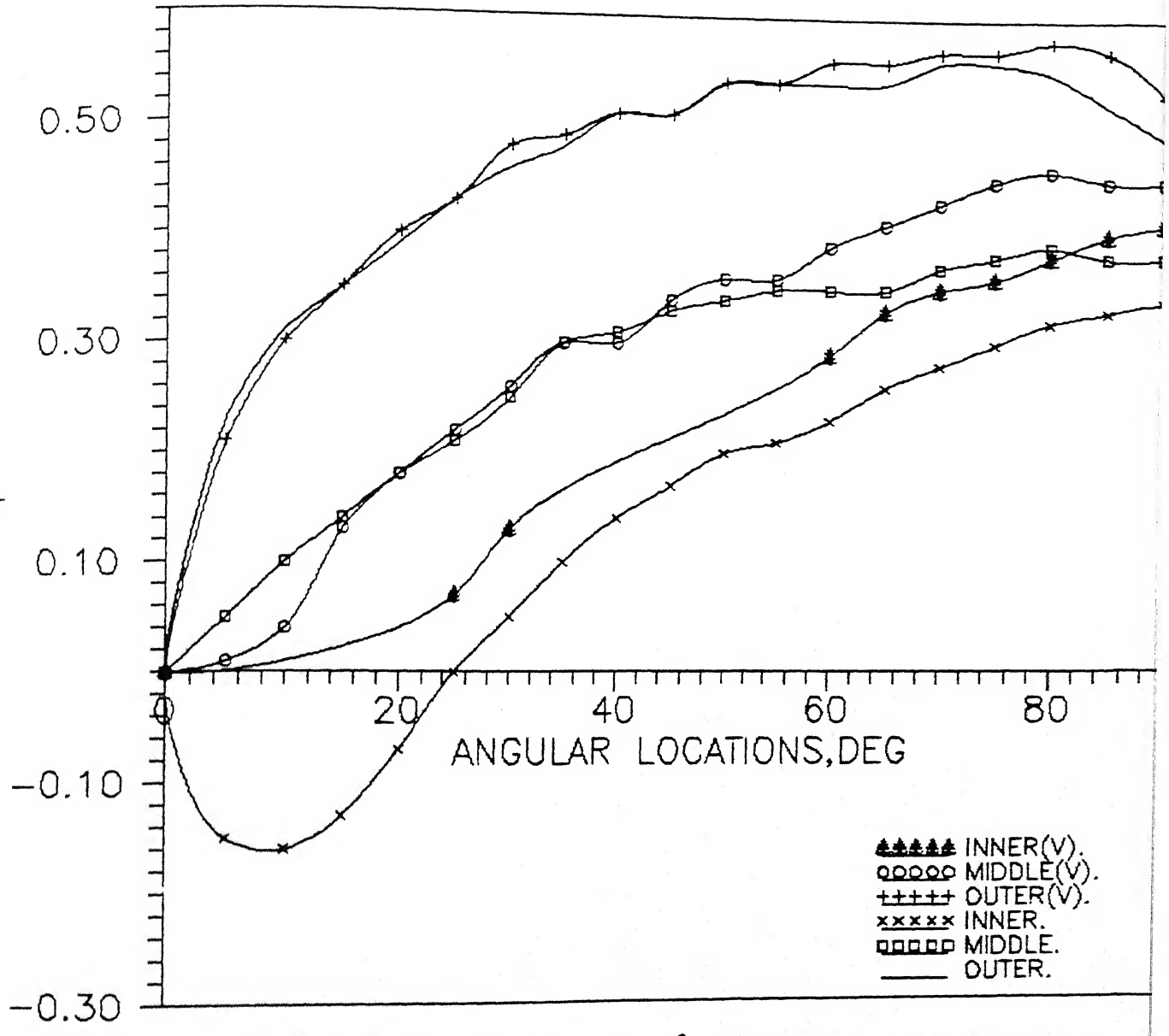

FIG.29 C_p DISTRIBUTION IN THE 4° DIFFUSER WITH VORTEX GENERATOR FROM 0° TO 22° & FROM 33° TO 55°.

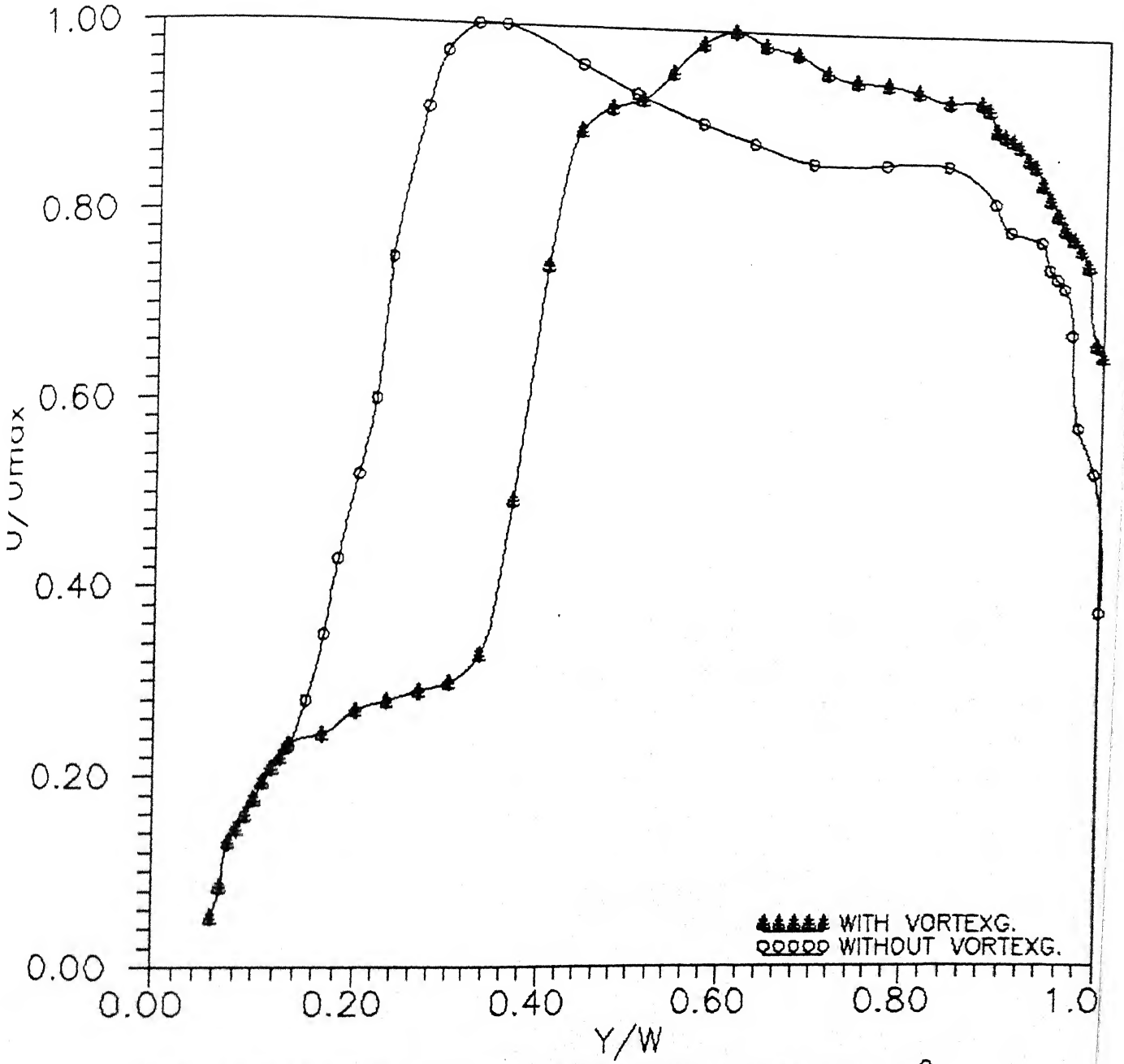

FIG.30 VELOCITY DISTRIBUTION (RADIAL) IN THE 4° DIFFUSFR(60°).

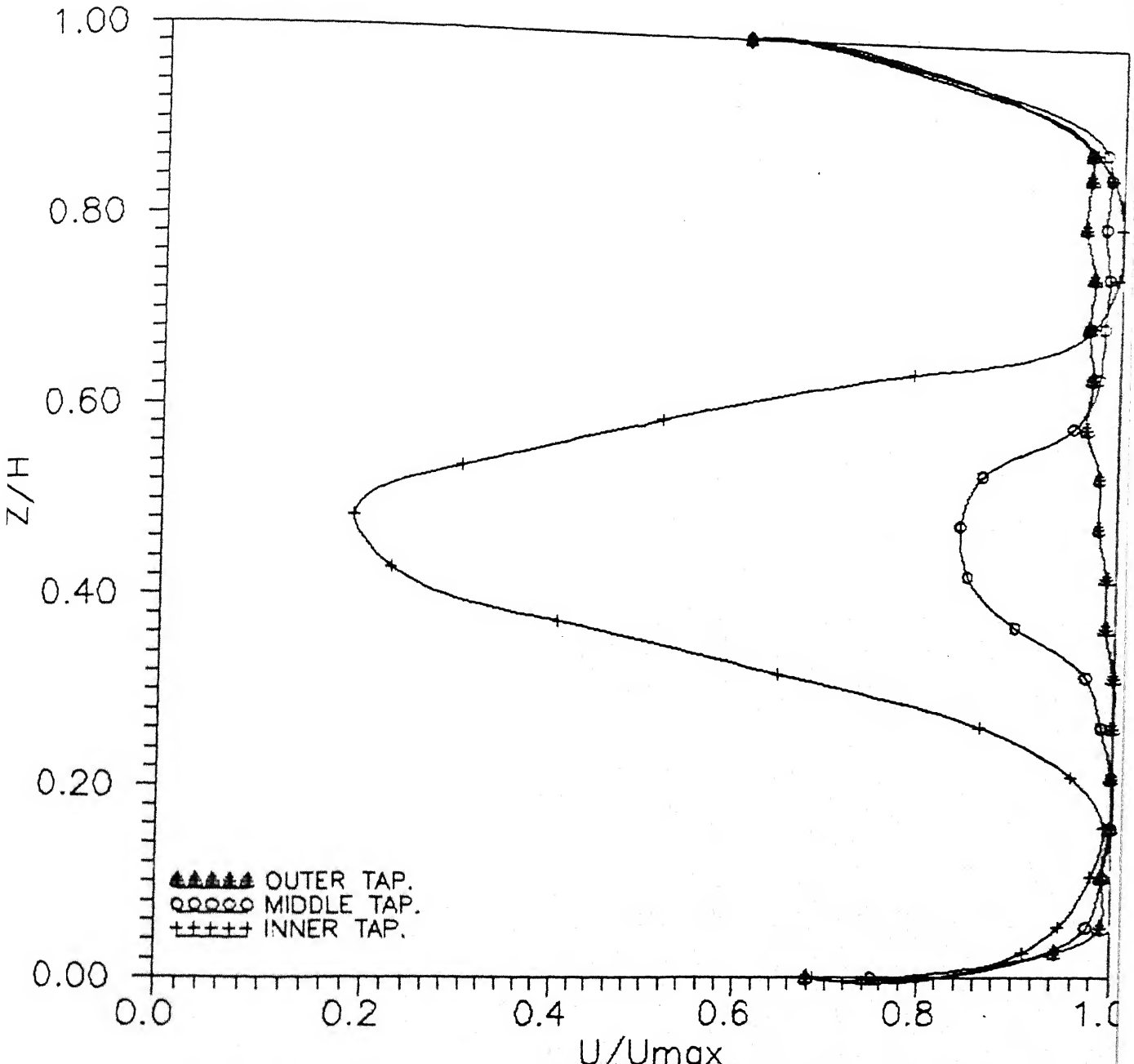

FIG.31 VELOCITY DISTRIBUTION(SPANWISE) IN THE 4^{0} DIFFUSFR(60^{0}) WITH VORTFX GFNFRATOR.

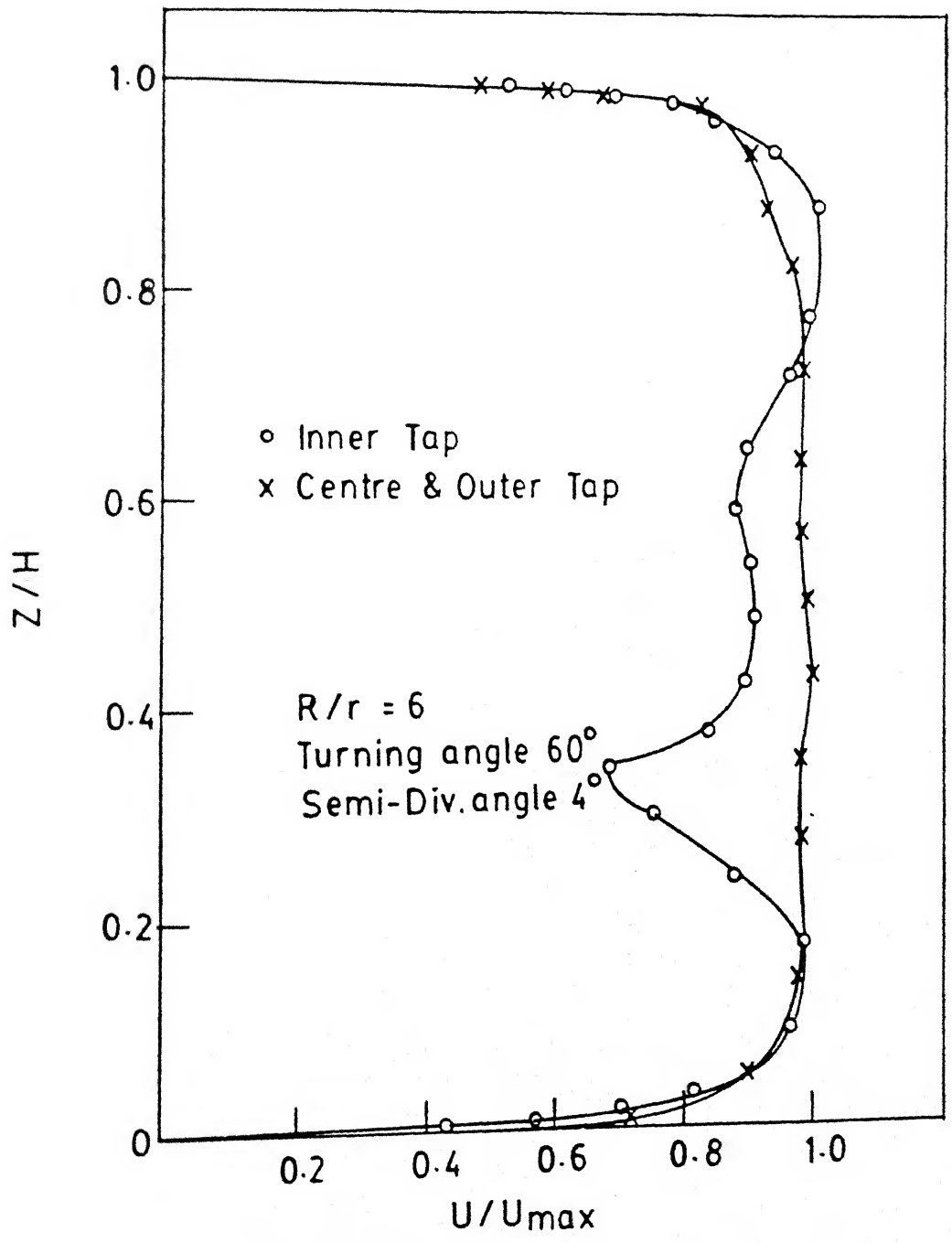

FIG.31a VELOCITY DISTRIBUTION (Spanwise)

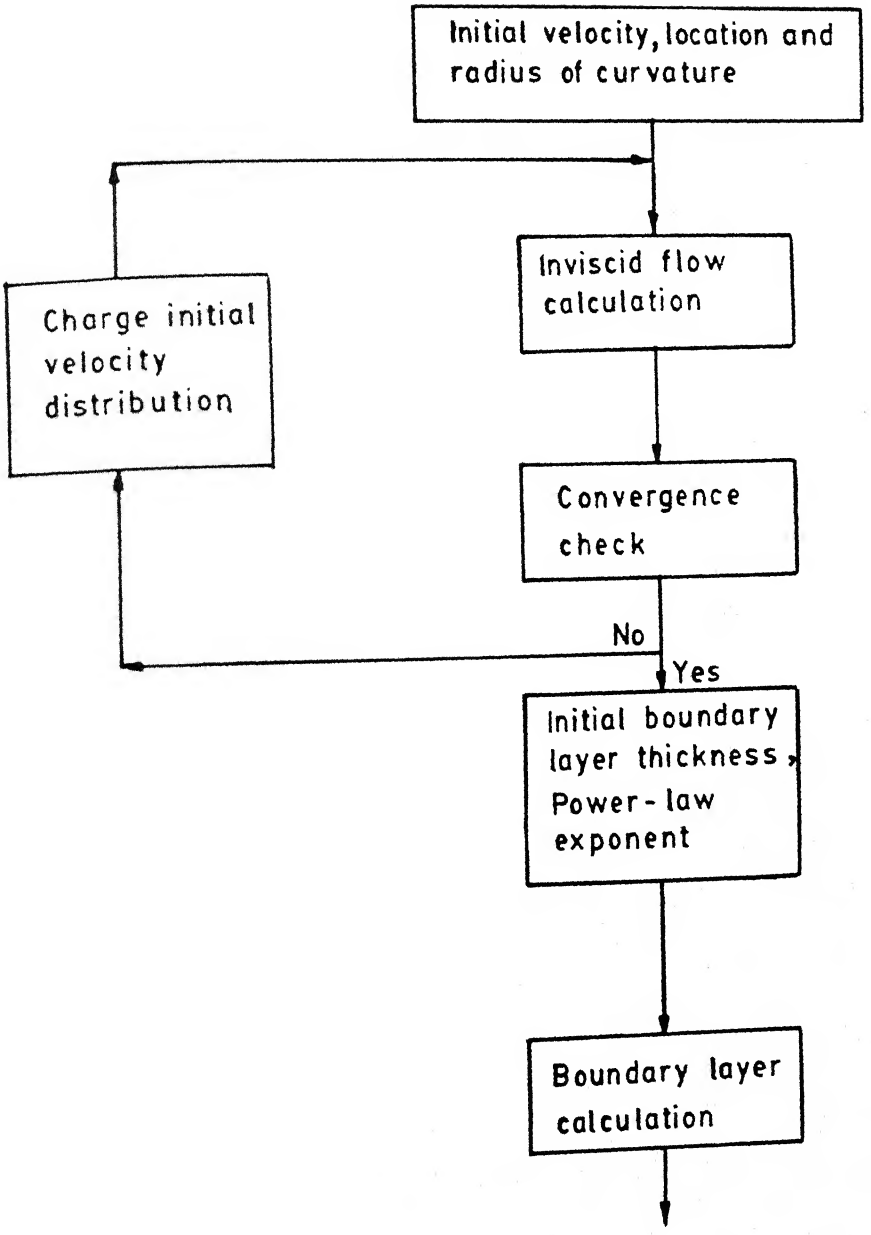

FIG. 32 COMPUTATION PROCEDURE

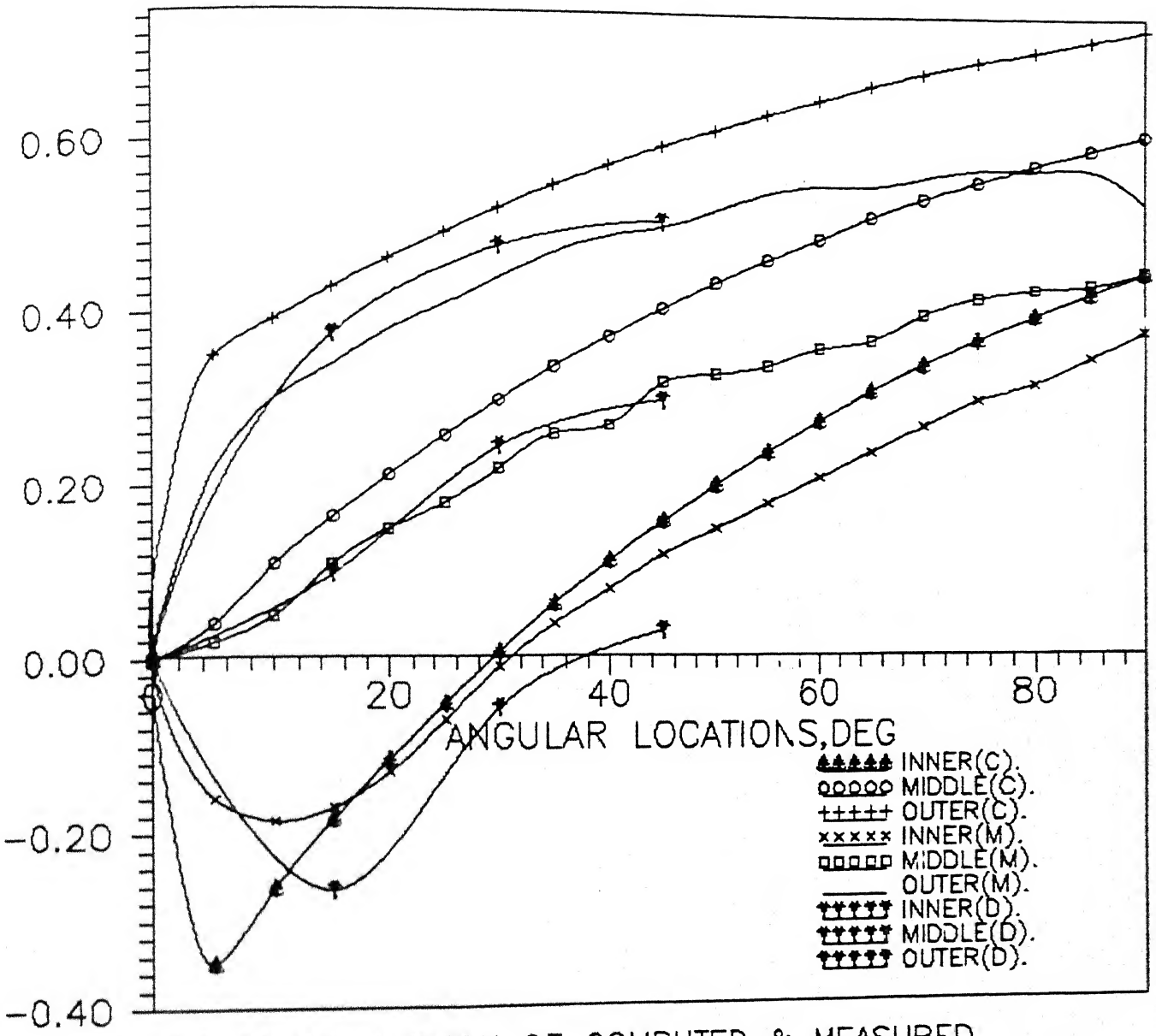

FIG.33 COMPARISON OF COMPUTED & MEASURED Cp DISTRIBUTION IN THE 3° DIFFUSER.

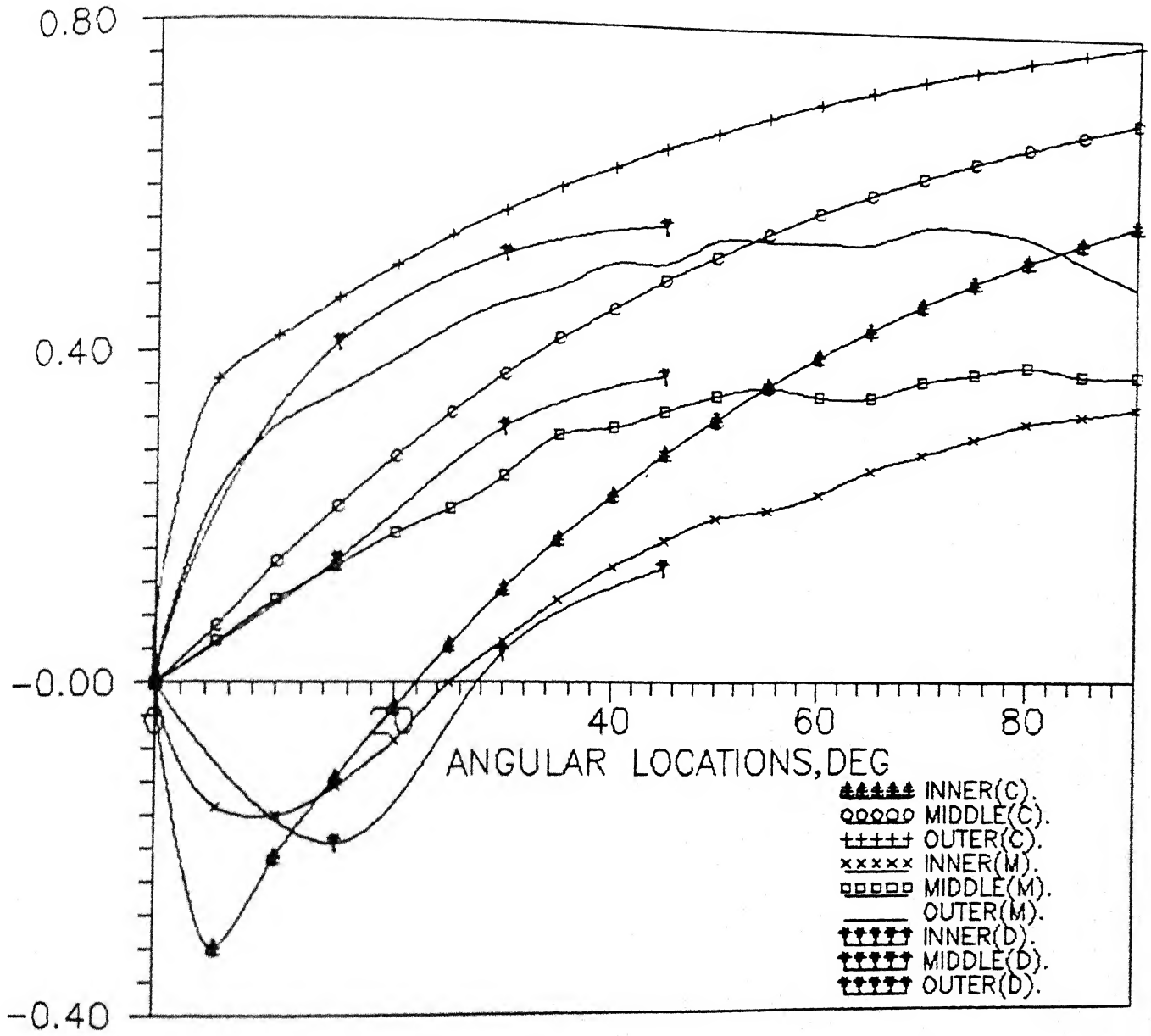

FIG.34 COMPARISON OF COMPUTED & MEASURED Cp DISTRIBUTION IN THE 4° DIFFUSER.

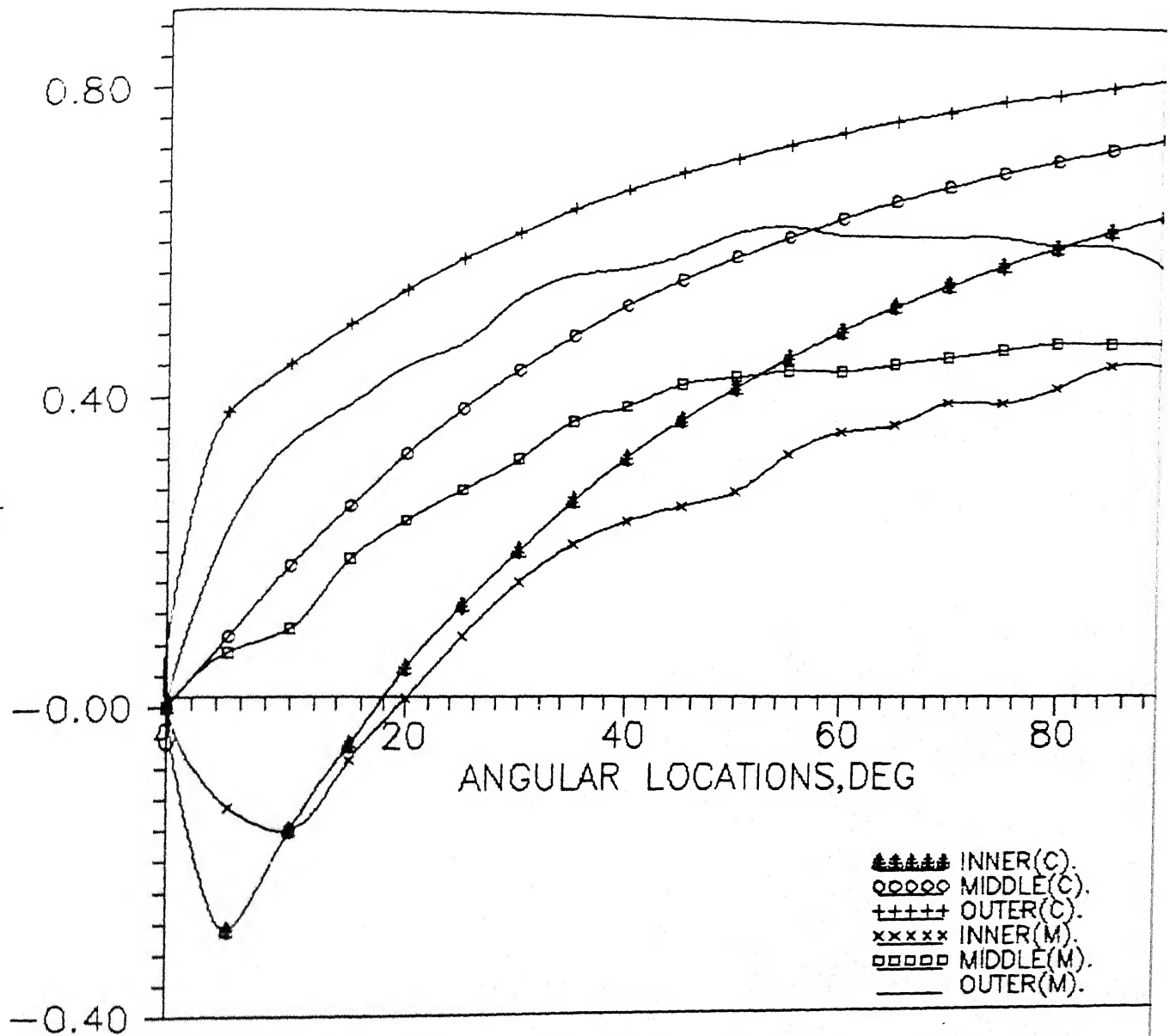

FIG.35 COMPARISON OF COMPUTED & MEASURED Cp DISTRIBUTON IN THE 5^0 DIFFUSER.

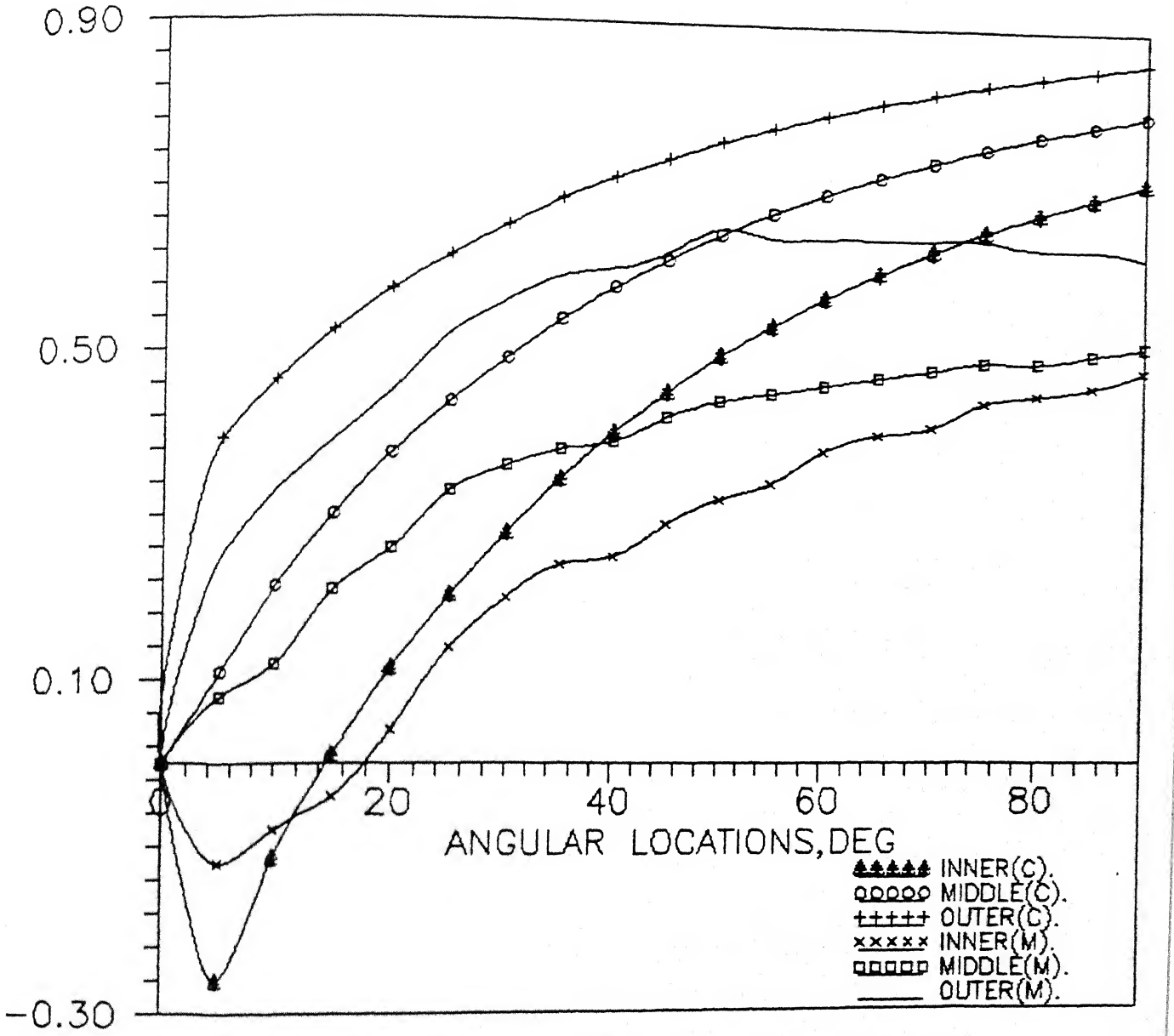

FIG.36 COMPARISON OF COMPUTED & MEASURED Cp DISTRIBUTION IN THE 6° DIFFUSER.

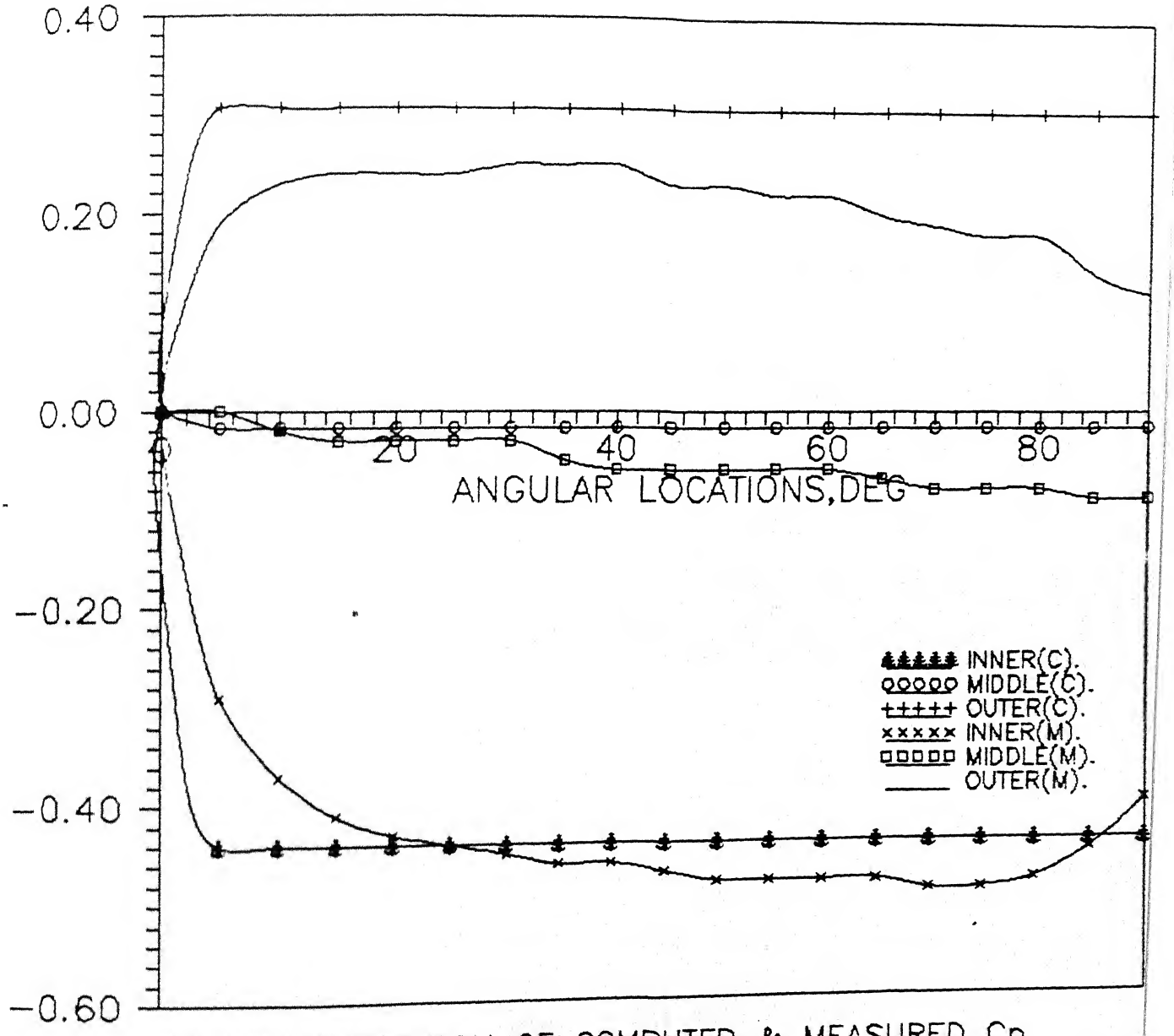

FIG.37 COMPARISON OF COMPUTED & MEASURED Cp DISTRIBUTION IN THE CURVED DUCT (R/r=6).

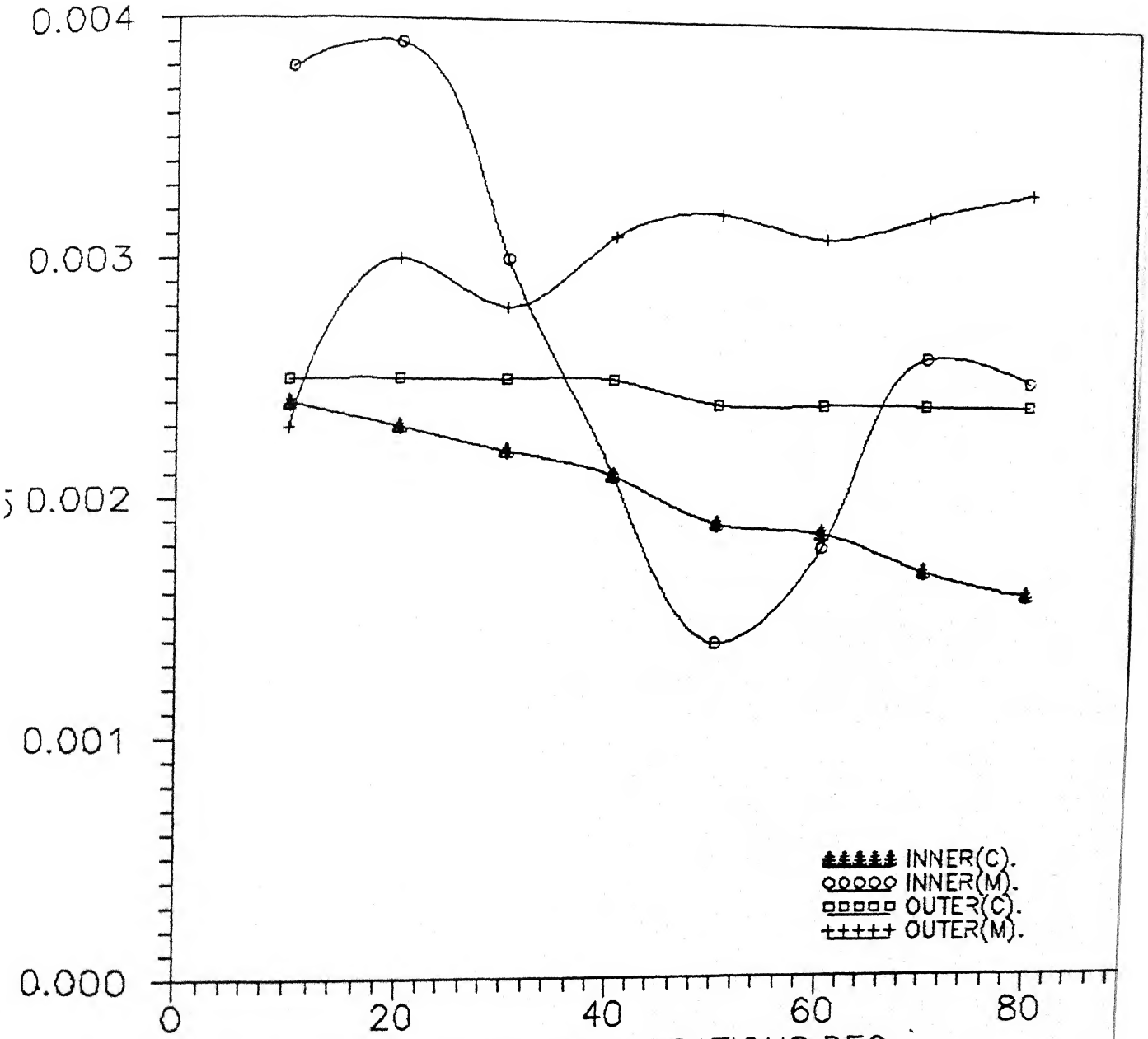

FIG.38 COMPARISON OF COMPUTED AND MEASURED Cf DISTRIBUTION IN THE CURVED DUCT.

AE-1991-M-JOH-FLO